INSTITUTO SUPERIOR TÉCNICO
Universidade Técnica de Lisboa

Helium and Hydrogen Permeation Experiments with MFI Zeolite Membranes for Tritium Processes

Maria Teresa Ramalho Tomé Parracho

Dissertação para obtenção do Grau de Mestre em

Engenharia Química

Júri

Presidente: Professor Sebastião Manuel Tavares da Silva Alves
Orientadores: Professora Maria Diná Ramos Afonso (IST)
Doutor David Demange (KIT)
Vogal: Professor Vítor Manuel Geraldes Fernandes

Maio de 2011

Acknowledgements

Firstly, I would like to thank to Karlsruhe Institute of Technology, for the opportunity that was given to me and for providing all the conditions that I needed to develop my thesis. I would like to express my gratitude to my supervisor at Karlsruhe Institute of Technology, Dr. David Demange, for his commitment, availability and all the support given whenever I needed. I would also like to thank to my supervisor at Instituto Superior Técnico, Prof. Diná Afonso, for all the availability, interest and support.

I would like to thank to Olga Borisevich for all the help and support, to Stefan Welte for teach me and help me in the lab, and to all the colleagues with whom I worked during my internship, for providing the best possible working environment and for their friendship.

A very special thank you to Diogo Oliveira, for understanding and encouraging me to perform the internship abroad, and for the unconditional support during my placement.

To my family, who has been present in every moment, thank you for the encouragement and support.

Abstract

Tritium (radioactive hydrogen) used in future fusion machines will be produced in the breeder blanket and recovered from huge helium throughputs by the Tritium Extraction System. As an alternative to the conventional technology, i.e. adsorption / desorption in a semi-continuous mode, the Tritium Laboratory Karlsruhe (TLK) has recently proposed a combination of a catalytic membrane reactor with a pre-separation and a pre-concentration stage using membranes. From tritium compatibility and performances points of view, zeolite membranes have been identified as promising candidates.

An advanced nanocomposite-MFI zeolite (nomenclature of the International Zeolite Association) membrane was experimentally investigated. The set-up to accommodate the membrane was built and commissioned. The permeance of single gases, helium and hydrogen, was measured for different temperatures using the dead-end method: opening the permeate side to the atmosphere and applying a transmembrane pressure, the permeate flow rate was measured and the permeance was calculated. Such unprecedented experiments at TLK revealed several problems (residual water in the membrane, loose tightness of the module) that have been solved during this study.

For helium, the maximum permeance was obtained at 400ºC (1.1 µmol/m^2.s.Pa) while for hydrogen the higher permeance was obtained at 350ºC (2.7 µmol/m^2.s.Pa). The ideal selectivity for hydrogen/helium was calculated and two maxima (α = 2.4) were obtained at room temperature and 300ºC. The membrane was operated for 300 h, including 20 h at 400ºC showing that such newly developed nanocomposite-MFI membranes are mechanically strong and thermally stable. Furthermore, the performances measured (permeance, ideal selectivity) seem appropriate for a multi-stage operation in the breeder blanket of the fusion machines.

Key-words: Tritium Extraction System, Zeolite Membrane, Dead-end Method, Permeance, Ideal Selectivity.

Resumo

O Trítio (hidrogénio radioactivo), que irá ser utilizado nas futuras máquinas de fusão nuclear, será produzido no *breeder blanket* das máquinas de fusão e recuperado de uma corrente de hélio pelo Sistema de Extracção de Trítio. Em alternativa às tecnologias convencionais, i.e. adsorpção / desorpção em modo semi-contínuo, o Tritium Laboratory Karlsruhe (TLK) propôs recentemente a combinação de um reactor catalítico de membrana com uma etapa de pré-separação e pré-concentração utilizando membranas. Do ponto de vista da compatibilidade com o trítio e de desempenho, as membranas zeolíticas foram identificadas como candidatas promissoras para a etapa de pré-separação pré-concentração.

Uma membrane zeolítica de nanocompósito-MFI (nomenclatura de acordo com a International Zeolite Association), foi estudada experimentalmente. Para tal, o equipamento para instalar a membrana foi construído. A permeância de gases simples, hélio e hidrogénio, foi medida para diferentes temperaturas usando o método "dead-end": abrindo o lado do permeado para a atmosfera e aplicando uma pressão através da membrana, o caudal de permeado foi medido e a permeâcia calculada. Esta experiência sem precedentes no TLK revelou vários problemas (água residual na membrana e vedação do módulo) que foram resolvidos durante este estudo.

Para o hélio, a permeância máxima foi obtida a 400ºC (1.1 μmol/m^2.s.Pa), enquanto que para o hidrogénio a permeância máxima foi obtida a 350ºC (2.7 μmol/m^2.s.Pa). A selectividade ideal hidrogénio/hélio foi determinada e obtiveram-se dois máximos (α=2.4) à temperatura ambiente e a 300ºC. A membrana operou durante cerca de 300 h, durante 20 das quais operou a 400ºC, o que mostra que esta membrana é mecanicamente resistente e termicamente estável. Além disso, o desempenho medido (permeância e selectividade) mostram que a membrana parece apropriada para operar nas máquinas de fusão.

Palavras – chave: Sistema de Extracção de Trítio, Membrane zeolítica, Método dead-end, Permeância, Selectividade ideal.

Table of Contents

Index of Tables

Index of Figures

List of abbreviations

AC – Adsorption Column

CMSB – Cryogenic Molecular Sieve Bed

CPS – Coolant Purification System

DEMO – Demonstration Power Plant

HTO – Highly Tritiated Water

ITER – International Thermonuclear Experimental Reactor

IZA – International Zeolite Association

JET – Joint European Torus

KIT – Karlsruhe Institute of Technology

RB – Reducing Bed

TBM – Test Blanket Modules

TES – Tritium Extraction System

TLK – Tritium Laboratory of Karlsruhe

Nomenclature

D – Diffusion Coefficient (m^2/s)

J – Flux ($mol/m^2.s$)

L – Membrane Thickness (m)

P – Permeance ($mol/m^2.s.Pa$)

p – Pressure

S – Solubility Coefficient ($mol/m^3.Pa$)

s – Selectivity or Separation Factor

α – Ideal selectivity or Permselectivity

Π – Permeability (mol/m.s.Pa)

Introduction

In the beginning of the twenty first century, fossil fuels provided about 85 percent of the total energy used around the world. With a growing world population, an increasing economic development worldwide and a rapidly depleting supply of fossil fuels, nuclear energy must be considered for the future as it offers the prospect of a long-term, environmentally benign energy. Nuclear energy can be created through nuclear fission or nuclear fusion. Nuclear fission is currently used, however it shows some drawbacks related with the production of large radioactive waste and the depletion of uranium supply. Fusion can solve these problems since it produces significantly less radioactive waste and the fuels used, deuterium and tritium, are easily available.

ITER (International Thermonuclear Experimental Reactor) is a joint international research project that aims to demonstrate the feasibility of using fusion as an energy source. ITER will be a fusion machine that is designed to produce ten times the power it consumes. ITER will be a bridge to a first fusion plant that will demonstrate the large-scale production of electrical power: the Demonstration Power Plant – DEMO. As for the fuel to the fusion reaction in the future fusion machines Tritium and Deuterium will be used. Deuterium is an abundant resource on earth, but tritium must be produced within the breeder blanket of the fusion machines. An important stage in the fuel cycle is the Tritium Extraction System (TES), which extracts tritium from the blanket to be re-injected in the fusion machine. A first concept for TES has been experimentally validated for ITER.

TLK (Tritium Laboratory Karlsruhe), Germany, has proposed an alternative TES based on the combination of membranes and membrane reactor, the PERMCAT, in order to facilitate the tritium management. The PERMCAT is a Pd-based membrane reactor that allows recovering tritium efficiently from any chemical species and producing a pure hydrogen stream enriched in tritium. To optimise the whole process, a combination of this membrane reactor with a pre-separation and pre-concentration stage using membranes is advantageous. A preliminary investigation has shown that newly developed zeolite membranes could be competitive for tritium processes in the breeder blanket since they are tritium compatible, chemically stable and withstand high temperatures.

This work was carried out during a seven months internship at Karlsruhe Institute of Technology (KIT) Germany, in the Cold Laboratory. The purpose of the work was to experimentally demonstrate that zeolite membranes can be used in the pre-concentration stage, obtaining experimental data on permeation and selectivity of a MFI zeolite membrane. The work was developed at lab scale without tritium. It consisted in the assembly of the experimental facility to accommodate the membrane, as well as performing measurements of the permeation fluxes and the selectivity of helium and hydrogen across the membrane.

This thesis is divided into three main parts. The first part includes a literature review on the subject in order to present the scope of this thesis to the reader. This chapter is divided in two parts. In the first part the fundamentals of fusion energy, the fusion roadmap and the tritium process in the breeder

blanket are described. In the second part a comprehensive explanation of the membrane processes and the zeolite membranes for gas separation processes are described.

The second part is the experimental part where the experimental set-up and instrumentation used as well as the methods used to carry out this work are described.

The third and final part addresses to the results obtained followed by a discussion where the results are explained and compared to literature data. At last, the final conclusions of this study are presented and some future perspectives are proposed.

PART I – LITERATURE REVIEW

1. Fusion Energy

Fusion energy is generated by nuclear fusion reactions. In these kind of reactions, two light atomic nuclei fuse together to form a heavier nucleus releasing a large amount of energy [1]. Fusion does not just happen. The atoms nuclei have an electric charge, and equal signal charges repel. But if two nuclei manage to get close enough together instead of repelling eachother, another force manifests itself: the nuclear force [2]. For such a reaction to occur, the reacting nuclei need to have enough kinetic energy to overcome the repulsive electrostatic barrier between the two of them. As the nuclear force is extremely powerful, the two nuclei are pulled together with a great force, and a new atom is born.

1.1 Fusion Reactions

There are several types of fusion reactions. In the sun, the process of fusion is known as the proton-proton chain. It starts with protons, and through a series of steps, they turn into helium. But in the sun massive gravitational forces create enough confinement energy for the nuclei to fuse. However, on Earth other confinement is needed (magnetic or inertial). Figure 1 shows three fusion reactions that can preferentially occur on earth. It is shown that fusion reaction rate rapidly increases with temperature until it maximizes and then gradually drops off. The Deuterium-Tritium rate peaks at a lower temperature (about 70 keV or 800 million Kelvin) and at a higher rate than the other reactions [3] therefore, the reaction between deuterium and tritium is the most favourable.

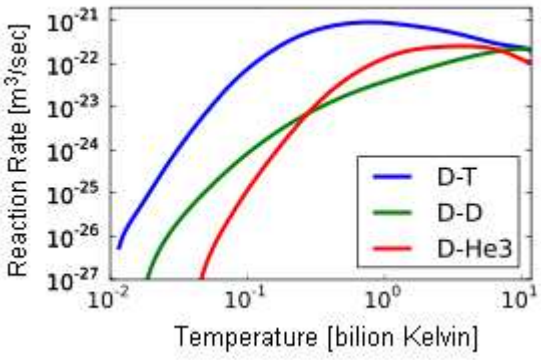

Figure 1– Reaction rate *versus* temperature for different fusion reactions [3].

- **Conditions for Fusion Reactions**

So that fusion can be used for energy production, three parameters, plasma temperature, density and confinement, need to be simultaneously optimized:

- Fusion reactions occur at a sufficient rate only at very high temperatures – up to several million of Kelvin. At such high temperatures, matter remains in plasma state that can be described as an 'electrically-charged gas' in which the negatively charged electrons in atoms are completely separated from the positively charged atomic nuclei [4].

- The number of fusion reactions per unit volume is proportional to the square of the plasma density. Therefore, the density of fuel ions must be sufficiently large for fusion reactions to take place at the required rate.

- Since the plasma comprises charged particles, powerful magnetic fields can be used to isolate the plasma from the walls of the vessel, thus enabling the plasma to be heated to temperatures up to 100 million Kelvin. This confinement of plasma reduces the conductive heat loss through the vessel walls. The most advanced confinement system is the Tokamak [5]. In a Tokamak the plasma is held in a toroidal vessel. Using special coils, a magnetic field is generated, which causes the plasma particles to run around in spirals, without touching the chamber wall. Figure 2 shows the magnetic system of a Tokamak.

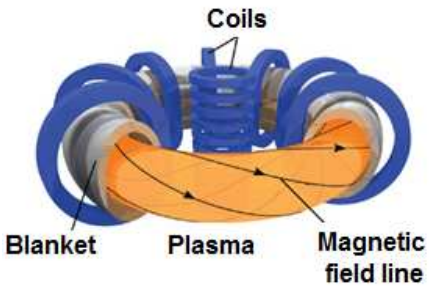

Figure 2 – Magnetic system of a Tokamak [2].

1.2 Fusion Roadmap

Research in nuclear fusion has been carried out during the last fifty years and scientific and technological progress has been made. In 1968, Russian scientists developed the Tokamak which quickly replaced other existing configurations. Several Tokamaks of small dimensions were built in various countries: Germany, France, England, Italy, USA, Russia and Japan. These devices lead to a rapid progress of the fusion processes and before 1990, several Tokamaks of big dimensions have been developed. In 1988, France built the Tore Supra, a Tokamak offering superconducting toroidal magnets, which allowed the creation of a strong permanent toroidal magnetic field. This was the first step for a future fusion reactor operating in a continuous mode.

1.2.1 The Joint European Torus – JET

JET is currently the largest and most powerful Tokamak in the world and the only machine capable of operating with the fuel mixture of deuterium-tritium of the future commercial reactors [5]. It is based in Culham, Great Britain, and it is the central research facility of the European Fusion Programme [4]. JET was explicitly designed to study plasma behaviour in conditions and dimensions approaching those required in a fusion reactor. JET has produced significant fusion power, up to 16 MW. "Break-even" conditions, Q=1, were almost reached where Q represents the amount of thermal power that is generated by the fusion reactions, divided by the amount of external heating power. A value of Q smaller than 1 means that more power is needed to heat the plasma than is generated by fusion [6]. Furthermore, JET has demonstrated that fusion devices can be operated safely with tritium fuel and radioactive structures can be maintained and modified using remote handling techniques. Despite the progress continuously achieved, JET is not able to generate more energy than the input energy. In order to demonstrate the feasibility of nuclear energy on a reactor scale it would be necessary a larger and more powerful device. This is the purpose of ITER project, the next step in fusion research.

1.2.2 The International Thermonuclear Experimental Reactor – ITER

ITER is a joint international research and development project, that aims to demonstrate the scientific and technological feasibility of using fusion as an energy source on earth. Currently, the partners in this project are: European Union, Japan, Russian Federation, China, Korea, India and USA. ITER started to be built in 2009 in Cadarache, France and it is expected to become operational in 2019. ITER will be a machine of the Tokamak type in which the plasma is confined by strong magnetic fields. It is designed to produce ten times the power it consumes: $Q \geq 10$ [6] and it will allow the study of plasmas in conditions similar to those expected in an electricity-generating fusion power plant. Figure 3 reveals a cut-way of the ITER machine.

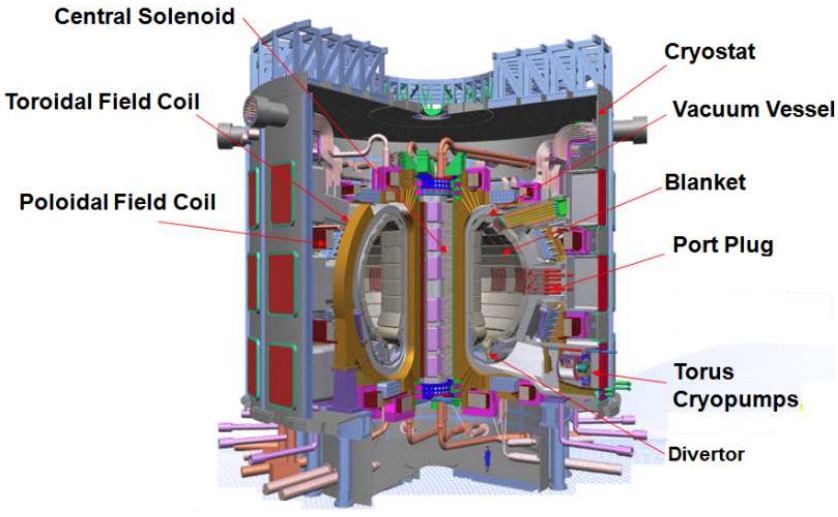

Figure 3 – The ITER machine. The man in the bottom shows the scale [6].

ITER will be the bridge towards a first plant that will demonstrate the large-scale production of electrical power and Tritium self-sufficiency: the Demonstration Power Plant – DEMO. While JET represents a pure scientific experiment, the reactor scale experiment ITER is designed to deliver ten times the power it consumes and DEMO is expected to be the first fusion plant to reliably provide electricity [5]. DEMO will be designed to produce up to 800 MW of electricity. DEMO is expected to begin operations in the early 2030s and the expectation is that after DEMO, the first commercial fusion power plant can be built. Figure 4 shows the advances made in fusion since 1988 and the path towards a reactor capable of producing electrical power from nuclear fusion reactions.

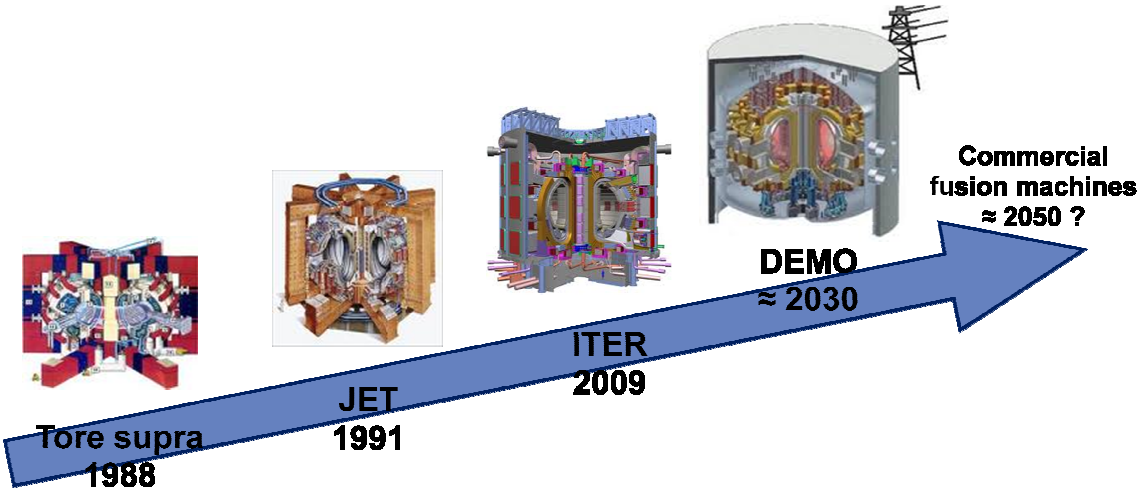

Figure 4 – Advances in nuclear fusion since 1988 and the path towards the nuclear fusion reactor.

1.3 Tritium Fuel Cycle

For the future fusion machines tritium self-sufficiency will be required. The tritium will be produced within the breeder blanket of the fusion machines. Since tritium is radioactive, special requirements for handling and processing it are necessary, for example the unspent tritium needs to be recovered and quantified. Two interconnected tritium loops will operate simultaneously as shown in Figure 5. The inner fuel cycle, in yellow, recycles and purifies the un-burnt tritium. The outer fuel cycle, in green, comprises the Tritium Extraction System (TES) and the Coolant Purification System (CPS). The TES extracts tritium from the breeder blanket to be re-injected, with negligible losses, to the ITER Tritium Plant for final processing. The Coolant Purification System (CPS) aims to remove the tritium that permeates from the breeder blanket, as well as the incondensable impurities, restraining the disposal into the environment. The instrumentation system, in orange, is required to ensure accurate and reliable tritium tracking between both cycles [7].

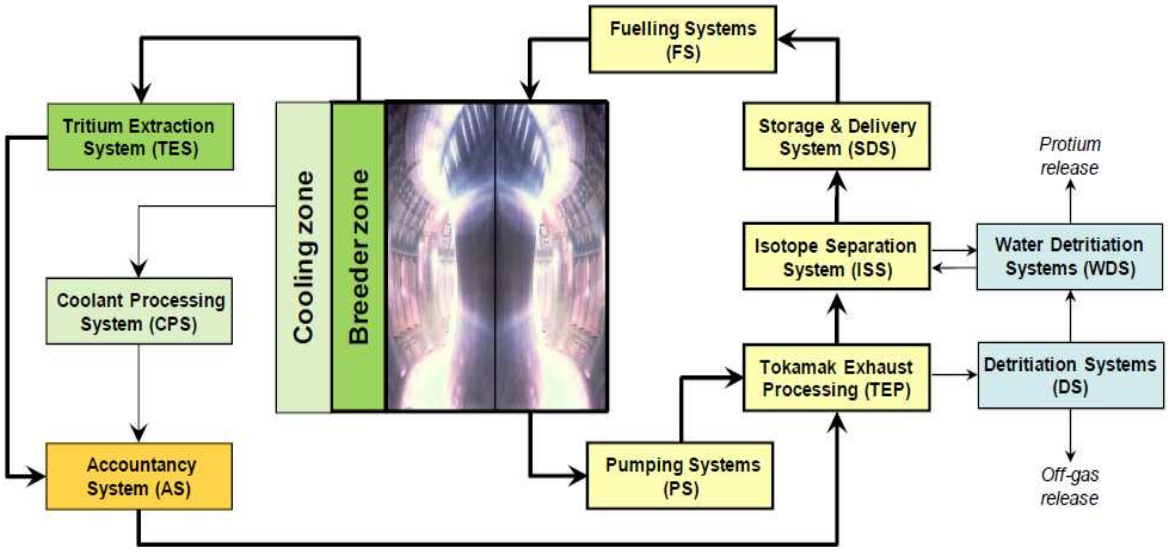

Figure 5 – Inner and outer tritium fuel cycles in future fusion reactors [8].

1.4 The Breeder Blanket

The fuel used for the fusion reaction in ITER is tritium and deuterium (two isotopes of hydrogen). Deuterium can be extracted from seawater in practically inexhaustible quantities. Tritium is continuously produced in the upper atmosphere although in very small quantities and it is also produced in CANDU reactors, about 100 g/year. All the available tritium will be consumed by ITER during its expected 20-year lifetime and DEMO will require 500 g/day to produce 800 MW of electrical power. Therefore, no sufficient external source of tritium will be available. But another source of tritium exists: it can be produced within the Tokamak, using a *breeder blanket*. Neutrons from plasma interact with lithium contained in the blanket that covers the interior surface of the vacuum vessel. Therefore, breeder blanket is a key component of the future fusion machines. The main functions of the breeder blanket are:

- Tritium production in the breeding zone (lithium pebbles will work as breeder and beryllium pebbles will work as neutron multiplier):

$$^{6}Li + neutron \rightarrow {}^{4}He + T + \Delta E$$
$$^{7}Li + neutron \rightarrow {}^{4}He + T + neutron + \Delta E$$

- Heat removal to produce electrical energy in the cooling zone
- Contribution to the shielding of the Vacuum Vessel and magnets

Figure 6 shows a schematic drawing of the breeder blanket for future fusion machines showing the different zones.

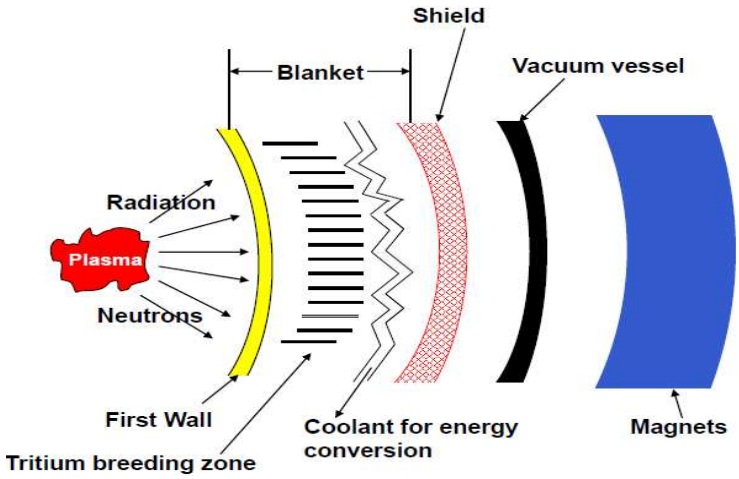

Figure 6 – Radial built of the breeder blanket for future fusion machines [9].

The ITER basic device has shielding, but no breeding blanket. It is foreseen that breeding blankets will be tested in small scale in ITER by inserting Test Blanket Modules (TBM) in specially designed ports. The TBM program aims to be the first integrated experimental demonstration of the principles of tritium self-sufficiency and critical experimental data on the feasibility, constraints and potential of the Deuterium-Tritium cycle for fusion systems will be obtained.

➢ Tritium Processes in the Breeder Blanket

For Demo, the tritium quantification is an important issue since an uncertainty in tritium inventory measurement will propagate errors in the tritium balance between both cycles. The tritium quantification is a difficult task since the levels to be measured are very low and tritium needs to be measured in different chemical forms either molecular or oxide. As the chemical forms and the tritium concentration depend on the Tritium Extraction System (TES), the process options for these systems need to be carefully studied. The tritium extraction will be managed by a helium gas stream of about 10^4 m^3/h doped with 0.1% of hydrogen. Table 1 shows the composition of the helium stream, with Q = Hydrogen, Deuterium or Tritium.

Table 1– Composition of the helium stream (extract).

Composition of the helium stream	
H_2	0,1 %
Q_2 (97% of all T)	4 ppm
Q_2O	4 ppm
Impurities	10 ppm

- **Tritium Extraction System (TES)**

A first TES concept for ITER TBM, has been experimentally validated for ITER operation. It is based on adsorption and it comprises an adsorption column (AC) for Q_2O removal from the purge gas stream, followed by a cryogenic molecular sieve bed (CMSB) for Q_2 removal, and a reducing bed (RB) that reduces Q_2O which allows transferring tritium only as Q_2 into the tritium plant avoiding handling Q_2O (highly tritiated water). A schematic diagram of the process is shown in Figure 7.

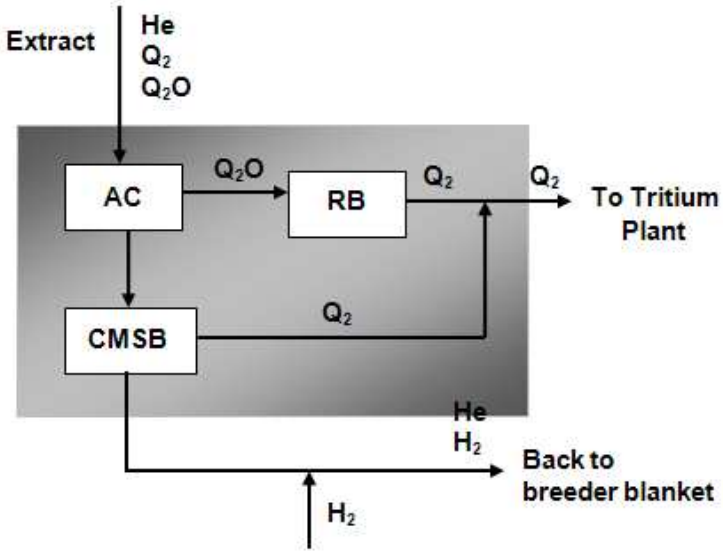

AC: Adsorption Column
RB: Reducing Bed
CMSB: Cryogenic Molecular Sieve Bed

Figure 7 – Current Tritium Extraction System experimentally validated for ITER.

Although this process is mature and workable at the ITER scale, it shows some disadvantages such as working at cryogenic temperatures, handling Q_2O and Q_2 for quantification and the fact that the application for DEMO is questionable due to the process complexity and size.

TLK has proposed an alternative for TES based on a combination of membranes and membrane reactor, the PERMCAT, in order to facilitate the tritium management. The PERMCAT is a catalytic membrane reactor that uses a dense metallic membrane based on palladium and operates on counter-current mode, that allows recovering tritium efficiently from any chemical species, by isotopis swamping, producing a stream enriched in tritium. To optimize the whole process, a combination of this membrane reactor with a pre-separation and pre-concentration stage using zeolite membranes to remove tritium has been proposed. Such combination could improve the tritium processes and facilitate its quantification in DEMO [8]. Figure 8 shows schematically how the combination of membrane and membrane reactor could be operated.

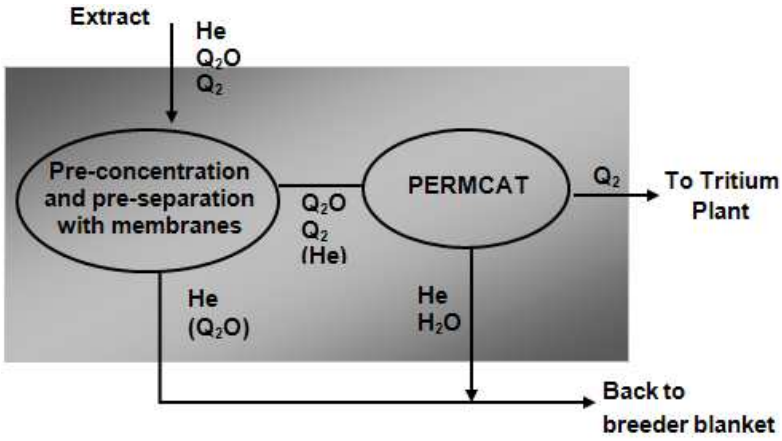

Figure 8 – Alternative TES using selective membrane and PERMCAT reactor proposed by TLK.

The membranes recycle to the breeder blanket the helium stream depleted in tritium and the PERMCAT processes the enriched stream containing highly tritiated water. Detritiated water returns into the breeder blanket, and the tritium recovered is routed as a continuous pure and enriched Q_2 stream into the inner-fuel. The main advantages will be working at non-cryogenic temperatures, it is a simple process and facilitates the tritium quantification.

Although the dense metallic membranes based on palladium, brings great advantages when integrated in PERMCAT reactor, they are not really appropriate for the pre-separation and pre-concentration step. The breeder blanket gases contain mainly helium and traces of tritium and the d-based membranes are not suitable to recover the tritium from the helium. A preliminary study as shown that newly developed zeolite membranes could be competitive for tritium process in the blanket [8]. Therefore, to test the process, this study was carried out using a MFI zeolite[1] membrane.

[1] Zeolites are usually classified, according to their symmetry, with a three-letter code assigned by the International Zeolite association (IZA).

2. Membrane Processes

During the past few decades membrane separation processes have undergone a rapid growth especially due to their inherent advantages which include low operating costs, low energy requirement and ease of operation. Currently, membrane processes can be found in a wide range of applications, such as biomedicine, water purification, waste treatment and food processing [10].

A membrane can be defined as a permeable or semi-permeable and selective barrier, that under a given driving force restricts the motion of certain species. Membrane processes are characterized by the split of a feed stream, that may be gaseous and/or liquid mixture or solution, into two different streams. The stream rejected by a membrane is called retentate and the stream passing through the membrane is termed permeate. A schematic diagram of a membrane process is shown in Figure 9.

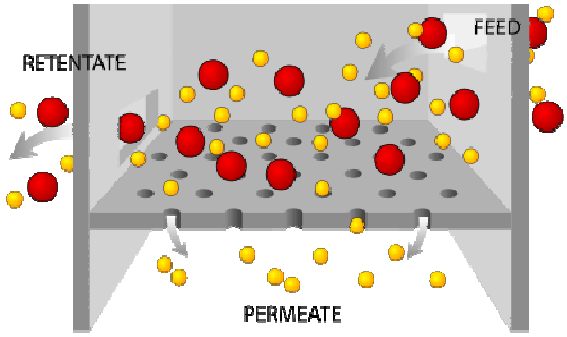

Figure 9 – Schematic diagram of a membrane process [11].

The key parameters that define the performance of a membrane are the flux, the permeance and the selectivity or separation factor. Flux is the molar flow rate of fluid passing through the membrane per unit area of membrane; it has units of [mol area^{-1} time^{-1}]. The higher the flux of a membrane at a given driving force, the lower is the membrane area required for a given feed flow rate and the lower are the capital costs of a membrane system. The permeance is the flux per unit pressure difference and has units of [mol area^{-1} time^{-1} pressure^{-1}]. Selectivity is a measure of the relative permeation rates of different components through the membrane. Tipically, membranes with high permeances show low selectivities.

The transport through the membrane occurs whether a driving force across the membrane exists, such as pressure, concentration, thermal or electrical potential gradient. Different driving forces lead to different membrane processes. There are eight major membrane processes which are widely used in industrial applications. They are microfiltration, ultrafiltration, nanofiltration, reverse osmosis, electrodialysis, dialysis, pervaporation and gas separation. The nature of the membrane, its structure and material, determine the type of application.

2.1 Inorganic Membranes

Membranes can be manufactured from a wide variety of organic and inorganic materials. Currently, the vast majority of commercial membranes are made from polymers. However, the efficiency of polymeric membranes decreases with time due to fouling, compaction, chemical degradation and thermal instability. Due to these drawbacks, polymeric membranes have not found application in separation processes where hot reactive gases are present [12].

Recently, intense research efforts have been made in the development and improvement of inorganic membranes in particularly for processes in which temperature, pressure or chemical environment prevent the use of polymeric membranes. In addition, to their improved thermal, mechanical and chemical stability, inorganic membranes show other advantages such as possibility to be sterilized, tritium compatibility and biocompatibility displayed by some inorganic membrane materials. The main advantages and disadvantages of inorganic membranes compared with organic polymer membranes are listed in Table 2.

Table 2– Comparison of inorganic membranes with polymeric membranes [13].

Inorganic membranes: Pros	Inorganic membranes: Cons
Long-term stability at high temperatures	High capital costs
Resistance to harsh environments	Brittleness
Resistance to high pressure drops	Low membrane surface area per module volume
Inertness to microbiological degradation	Difficulty in achieving high selectivities in large scale microporous membranes
Easy regeneration after fouling	Generally low permeability of the highly selective (dense) membranes at medium temperatures
Easy catalytic modification	Difficult membrane-to-module sealing at high temperatures

2.1.1 Transport Mechanisms in Inorganic Membranes

According to their structural characteristics membranes can be classified into three main categories: dense (nonporous), porous and composite membranes.

Dense membranes are free of discrete, well-defined pores or voids. They consist of a dense film through which permeants are transported by solution-diffusion. The components separation is directly related to their relative transport rate within the membrane, which depends on the membrane material, the species to be separated and their interactions with the membrane. Thus, dense membranes can separate permeants of similar size if their concentration in the membrane material (that is, their solubility) differs significantly. Most gas separation, pervaporation, and reverse osmosis membranes use dense membranes to perform the separation. There are two main types of inorganic dense

membranes which are polycrystalline ceramic and metal. For example, dense metallic membranes based on palladium are used in some tritium processes.

Porous membranes have a rigid, well-defined static pore structure, which depending on the formation process can be highly connected and tortuous or nonconnected and straight. Pores in membranes can be classified according to their size as macropores (>50 nm), mesopores (2-50 nm) or micropores (<2 nm) [13]. Porous membranes consist of a porous wall or porous top layers (metal, oxide, glass) on a porous support of higher pore size which provides the required mechanical resistance. In general terms, as the pore size of the membrane increases, the permeability of the membrane also increases, but the membrane becomes less selective.

Composite membranes are made up of more than one material, often a combination of dense-dense or dense-porous membranes (for example metal-metal, metal-glass, metal-ceramic).

Various mechanisms for transport across the membranes have been proposed depending on the properties of both the permeant and the membrane. The transport across a membrane depends on the pressure and temperature, as well as on the pore size of the membrane and the properties of the permeating molecules (molecular weight, molecular size and heat of adsorption).

- **Solution-diffusion:**

Dense membranes allow substances to pass through them by a process of solution and diffusion that takes place in three consecutive steps: sorption of components from the feed mixture at the upstream membrane surface, diffusion of the absorbed components through the membrane matrix and desorption from the membrane at its downstream surface. This is also the classical transport mechanism for some polymeric membranes.

- **Molecular sieving:**

This mechanism assumes that only molecules of an appropriate size can permeate through the membrane. It takes place when the pores sizes of the membrane can discriminate between two or more species depending on their molecular size. In this case, the membrane acts like a sieve that only allows the permeation of species with a molecular size lower than the pores size [13].

- **Surface diffusion:**

It is a mechanism in which the molecules adsorbed on the pore wall diffuse on the porous surface due to a concentration gradient in the adsorbed phase. Usually, it takes place simultaneously with viscous flow [14].

- **Capillary condensation:**

This mechanism takes place when one of the constituents of a multi-component gas is a condensable vapour and the pores of the membranes are small enough. In such case the vapour adsorption proceeds to the point at which pore spaces are filled with liquid separated from the gas phase.

Therefore, selective mass-transport of just one of the species of the original mixture is achieved. This mechanism is highly selective, because the diffusion of non-condensable species ideally depends on their retention in the membrane pores.

- **Knudsen diffusion:**

In this case separation is achieved when the mean free paths of the molecules are large in comparison with the membrane pore radius. As a separation process this mechanism is limited to systems of large molecular weight ratios [14].

- **Viscous flow:**

Viscous flow is the flow of a gas through a channel under conditions where the mean free path is small in comparison with the cross section area of the channel, thus the flow characteristics are determined mainly by collisions between the gas molecules. It is a non-selective mechanism.

Figure 10 shows the mechanisms that can take place in different membranes.

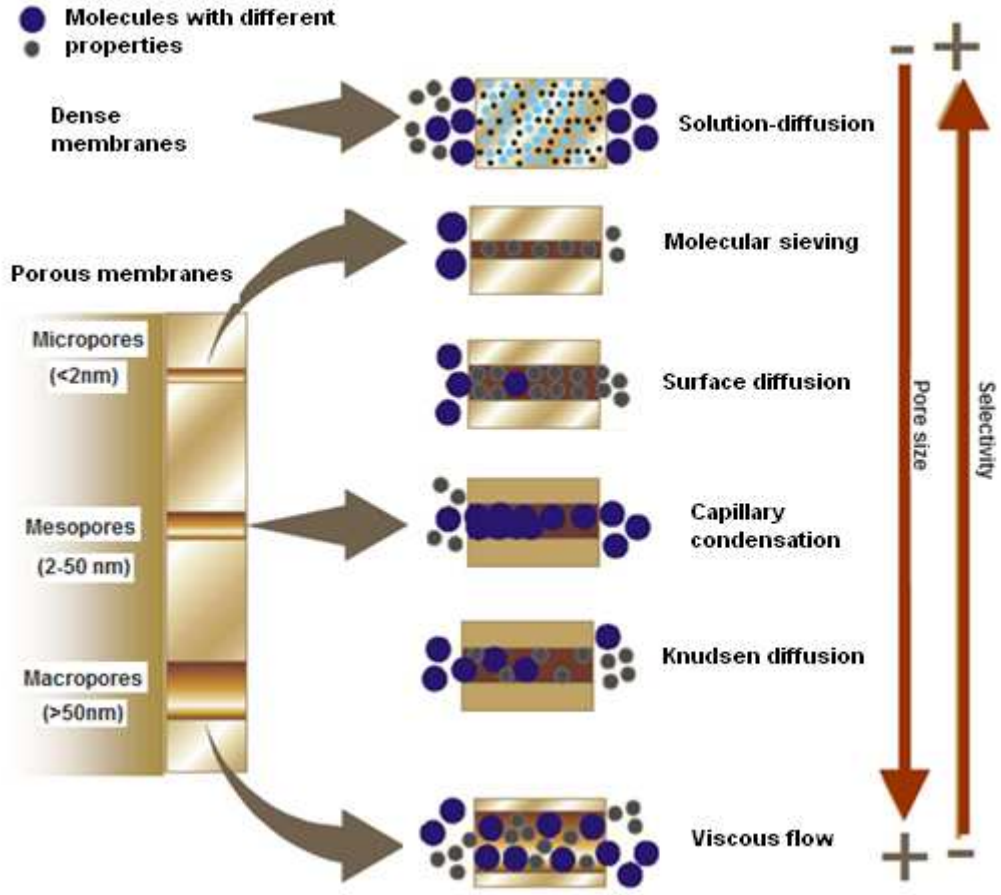

Figure 10 – Transport mechanisms in inorganic membranes [15].

2.1.2 Zeolite membranes

Zeolites are aluminosilicate crystalline materials which have a highly regular and open microporous (< 2 nm) structure [11]. The zeolite structure consists of a three-dimensional network of SiO_4 and AlO_4 tetrahedra linked to each other by shared oxygen atoms forming cavities or cages that can be connected by ring or pore openings of defined size and shape. The AlO_4 groups carry negative charge which is balanced by cations. The cations are mobile and can be exchanged by other cations. Zeolites are chemically represented by the empirical formula: $M_{2/n}O.Al_2O_3.ySiO_2.wH_2O$, where *y* is 2 to 10, *M* is the cation valence and *w* represents the water contained in the voids of the zeolite [16].

At present, about 132 different structural types of zeolite are known, each of them with its own distinct pore size, shape and interconnectivity [11]. The size of pores openings ranges from 0.3 nm to ~2 nm. The small and well-defined pore size gives the zeolite molecular sieving properties as well as a very high specific surface area, often several hundred square meters per gram. A molecular sieve is a material capable of separating components in a mixture on the basis of molecular size or shape. Figure 11 shows an example of a zeolite structure.

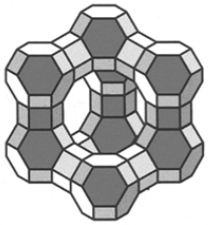

Figure 11 - Structure of MFI zeolite

The properties of zeolites depend on several parameters such as structure, Si/Al ratio and framework cations. By changing the Si/Al-ratio, the polarity of a zeolite can be adjusted. A lower Si/Al ratio gives a more hydrophilic zeolite, which strongly adsorbs polar molecules, therefore zeolites are widely used as drying agents. On the contrary, materials with low aluminum content, such as pure silica, have an hydrophobic nature. Zeolites exhibit advantageous properties such as molecular adsorption, catalytic activity and ion-exchange capacity.

The crystalline zeolite structure offers the opportunity to prepare thin, highly selective membranes. Due to a well-defined pore structure of molecular size and preferential adsorption properties, zeolite membranes are suited for separation processes. In general they are mechanically strong and thermally and chemically resistant. They can separate molecules based on their size and shape. The uniformity of their pore sizes ensures high selectivity, whereas the intrazeolite pore channel can be chemically modified to enhance adsorptive and diffusional selectivity for certain species [11].

An important feature of any membrane is a high selectivity, combined with a high flux. A membrane with a high selectivity but with a low flux is not attractive for practical application because the membrane area must be very large to handle a given feed flow rate. Besides good separation performances, reproducibility is another essential factor to put membranes in large scale application.

The inorganic nature of zeolite membranes enables them to withstand severe physical and chemical environments, and can be easily regenerated through ion exchange or thermal treatment. Currently, zeolite membranes find applications in areas as diverse as gas pervaporation, gas separation, membrane reactors, sensors, electrodes and corrosion protection coating.

- **Preparation of zeolite membranes**

Zeolite membranes can be prepared in three different ways: as self-supported zeolite film, as thin zeolite film on a mesoporous support, such as ceramic, glass or metal [11] or even dispersed inside porous support (the pore-plugging synthesis) [17]. Preparation of supported zeolite membranes is the most frequently used technique. This method provides the required mechanical resistance to the system and allows the growth of a selective zeolite layer. Supported zeolite membranes are more suitable for industrial applications because of the greater mechanical strength and thermal stability provided by the support material. Several strategies have been developed to prepare such zeolite membranes [11]:

Direct in situ crystallization without seeds: consists of placing a suitable support, such as stainless steel, silicon, quartz or ceramic support in direct contact with the synthesis solution;

Seeding-assisted crystallization: consists in pre-seeding the support with a layer of zeolite seed particles prior to the hydrothermal treatment.

Crystallization of a dry gel: in this technique, a dry gel that has been previously deposited on the surface of the support is transformed in a steam atmosphere into a continuous zeolite layer.

The pore-plugging synthesis consists in growing zeolite crystals within the support pores until their complete blocking by the zeolite material. Figure 12 shows a comparison between a supported zeolite membrane and the pore-plugging synthesis [17].

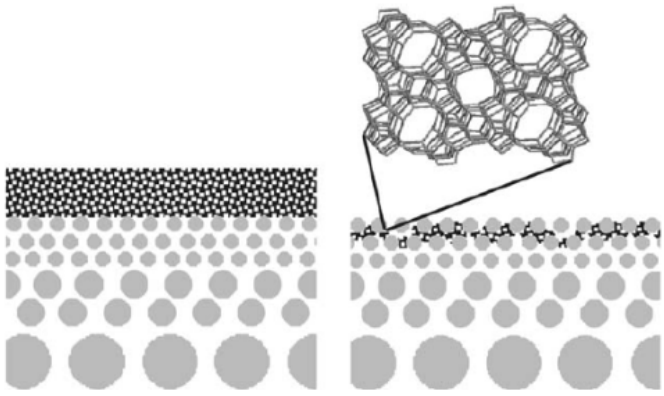

Figure 12 – Schematic comparison between self-supported zeolite film and pore-plugging synthesis [17].

The pore-plugging synthesis is a membrane preparation method not so commonly used. However, it has some advantages, such as having better thermal stability, lower equivalent thickness, higher reproducibility and they are easier to scale-up.

There are several types of defects in zeolite membranes, such as cracks, open grain boundaries and nonclosed film. It is not possible to eliminate all defects, because the zeolite film is polycrystalline. Nevertheless, it is important to minimize the defects concentration because flux through defects reduces the separation performance.

2.2 Membrane Gas Separation

Gas separation is a common and important operation widely employed throughout the chemical and gas processing industries. Conventional methods for gas separation, such as cryogenic distillation, absorption and adsorption are energy intensive due to high heating and cooling load and the units installation usually requires a very high capital cost. Over the past half century, there has been a great interest in alternative methods for gas separation in the industries and this has led to the development of membrane gas separation. The main advantages of gas separation membranes are the fact that they do not involve phase change, they are very easy to scale-up and they can be easily integrated with other separation units.

Membranes for gas separation are commercially available and in use for a variety of industrial applications. The main gas separation membrane applications are described in Table 3.

Table 3 – Membrane gas separation applications [12].

Common gas separation	Application
O_2 / N_2	Oxygen enrichment, inert gas generation
H_2 / Hydrocarbons	Refinery hydrogen recovery
H_2 / N_2	Ammonia Purge gas
H_2 / CO	Syngas ratio adjustment
CO_2 / Hydrocarbons	Acid gas treatment, landfill gas
H_2O / Hydrocarbons	Natural gas dehydration
H_2S / Hydrocarbons	Sour gas treating
He / Hydrocarbons	Helium separation
He / N_2	Helium recovery
Hydrocarbons / Air	Hydrocarbons recovery, pollution control
H_2O / Air	Air dehumidification

Membrane gas separation is a pressure-driven process, in which a gas mixture at high pressure is passed across a membrane that is selectively permeable to one component of the feed mixture; the permeate stream is enriched in this species. The degree to which the various constituents of a gaseous mixture can be separated by a membrane depends upon the mass-transport mechanism(s) present under given environmental conditions. The mass-transport mechanism(s) of the membrane

dictates the relative fluxes of the gaseous species, which in turn affect the membrane separating ability.

The performance and reliability of membranes for gas separation are improving. Membrane gas separation is becoming competitive with other technologies in a growing number of applications. The choice of the membrane material for gas separation applications is based on specific physical and chemical properties. The membranes properties depend upon the material (permeability, separation factors), the membrane structure and thickness (permeance), the membrane configuration (e.g., flat, hollow fiber) and the module and system design.

2.3 Membrane Permeability and Selectivity

A quantitative measure of the gas transport through the membrane is the flux, J (mol/m^2.s), which is defined as the number of moles that pass through a unit area per unit time. For low concentrations, the molar flux is given by Fick's first law,

$$J = -D\frac{dC}{dx} \tag{1}$$

where D is the diffusion coefficient (m^2/s) and dC/dx is the concentration gradient through the membrane. Assuming a constant concentration gradient across the membrane, the flux may be given approximately by:

$$J = D\frac{C_2 - C_1}{L} \tag{2}$$

where C_1 and C_2 are the downstream and the upstream concentrations, on the membrane surface, (corresponding to the pressures p_1 and p_2), respectively and L is the membrane thickness (m), as shown in Figure 13.

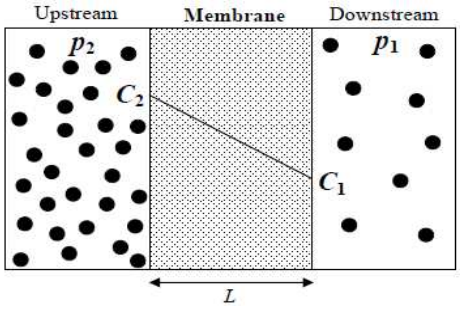

Figure 13 – Membrane gas separation with a constant concentration gradient.

The membrane performance is commonly reported in terms of permeance, P (mol/m².s.Pa), or permeability, π (mol/m.s.Pa), where:

$$\Pi = P \times L = \frac{JL}{p_2 - p_1} = \left(\frac{C_2 - C_1}{p_2 - p_1} \right) D \tag{3}$$

Whether the upstream pressure is much higher than the downstream pressure ($p_2 >> p_1$) and the permeate concentration is nearly null, the permeability can be simplified as:

$$\Pi = \frac{C_2}{p_2} D \tag{4}$$

At low concentrations Henry´s law directly relates the concentration C to the partial pressure p

$$C = S.p \tag{5}$$

where S is the solubility coefficient (mol/m^3.Pa). Thus, Eq. (4) becomes:

$$\Pi = SD \tag{6}$$

This expression is useful to envisage the permeability as the product of two components:

- Solubility, *S*, an equilibrium component describing the amount of gas molecules within the membrane;
- Diffusion, *D*, a dynamic component describing the mobility of the gas molecules within the membrane.

Another key membrane property is the selectivity. The ideal selectivity (single component selectivity) between components i and j is given by:

$$\alpha_{i,j} = P_i / P_j \tag{7}$$

For gas mixtures, the permeance of solute *i* is defined by:

$$P_i = \frac{J_i}{(p_{i2} - p_{i1})} \tag{8}$$

and the gas mixture selectivity or separation factor is given by the ratio of the molar fractions of the components *i* and *j* in the permeate stream (*y)* and in the feed stream (*x*) :

$$s_{ij} = \frac{y_i / y_j}{x_i / x_j} \tag{9}$$

An important difference between the ideal and the mixture selectivity is that the latter is assessed under actual mixture conditions, including the effect of competitive adsorption and interactions between species.

PART II – EXPERIMENTAL PART

1. Measurements of Zeolite Membrane Permeance

The zeolite membrane permeance for two different gases, helium and hydrogen, was measured using the dead-end method at different temperatures in order to identify ideal conditions to operate the membrane. Those gases were chosen to study the membrane performance since tritium is an isotope of hydrogen, helium will be the matrix in the process, and the main purpose of the zeolite membrane will be to separate the tritium from the helium stream.

To measure the membrane permeances for single gases there are three main simple methods that can be used:

- A batch technique, that is used for single component measurement, consists in bringing the feed side to an initial pressure and then shut off the supply. The transmembrane flux is then determined from the measurement of the transient pressure decline at the feed side during application of vacuum at the permeate side [19];
- Another batch technique, consists in applying a continuous flow at the feed side, while the permeate side is isolated after being evacuated. The measurement of the rising pressure at the permeate side provides the permeation flux through the membrane [19];
- The open system or dead-end method consists in apply a pressure difference across the membrane. The permeation flux is measured in the permeate side, maintaining the feed side at a higher pressure than the permeate side, which is usually at atmospheric pressure [19].

The first two techniques yield high permeances. However the second one takes a longer time to record a measurable decline of pressure at the feed side while the first one is faster because a low pressure build up at the evacuated permeate side can be easily and accurately measured. The open system method enables a fast test and accurate results and it is the simplest method since it needs less equipment and instrumentation.

1.1 MFI Membrane

This study focused on a nanocomposite MFI hollow-fibre membrane, in which the feed gas flows inside the channels and the permeate is collected outside. The membrane and respective module was provided by Institut des Recherches sur Catalyse et L'environnement de Lyon (IRCELYON). This membrane was synthesized via pore-plugging [17]. This synthesis method consists in growing the zeolite crystals within the pores of a ceramic alumina substrate, until complete blocking of the pores by the zeolite material. The result is a continuous composite zeolite-alumina membrane. This zeolite membrane synthesis method was combined with a new method that consists on a 9 hours interruption during hydrothermal synthesis in the nucleation and crystal growth process of the nanocomposite MFI-alumina material. This new method allows nutrient precursor moieties to diffuse into the support pores

and as a result a composite MFI alumina selective layer is obtained [18]. Figure 14 shows a picture of the hollow fibre MFI-nanocomposite membrane used, which is fixed and hosted inside a porous holder. The characteristics of the membrane are described in Table 4.

Figure 14 – Nanocomposite-MFI alumina hollow fibre membrane used in this study.

Table 4 – Characteristics of the Nanocomposite-MFI zeolite membrane [33].

Structural parameters of the zeolite membrane	
Geometry	Hollow Fiber
Zeolite structure	MFI
Length (cm)	13
Effective surface area for mass transfer (cm^2)	4,97
Thickness (μm)	<1

1.2 MFI Membrane Module

The membrane is operated inside a suitable stainless steel module equipped with hoses for feed, permeate, retentate and sweep gas. A picture of the module and respective hoses is shown in Figure 15 whereas Figure 16 shows a schematic drawing of the permeation module.

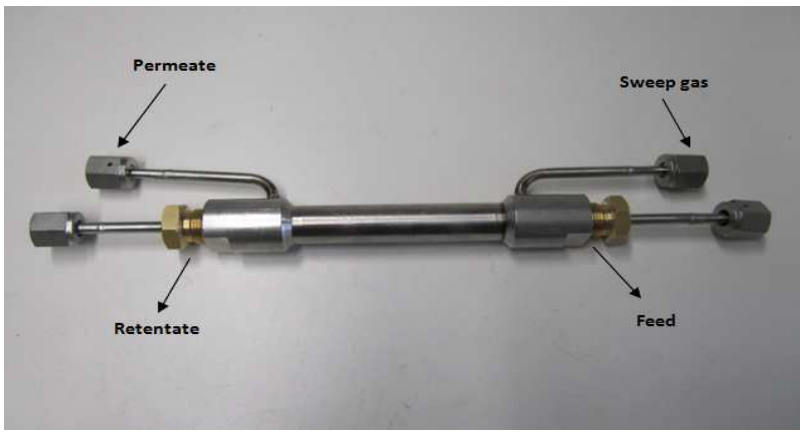

Figure 15 - MFI membrane module and respective hoses.

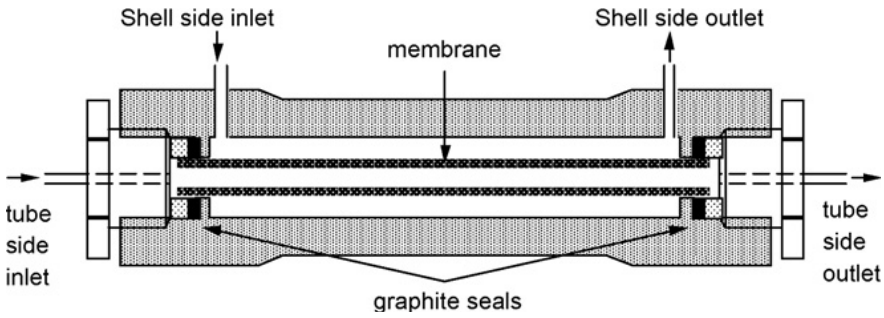

Figure 16 – Schematic drawing of the permeation module, showing the nanocomposite MFI-ceramic hollow fibre membrane unit sealed inside the module with graphite seals.

1.3 Experimental Set-up for Single Gas Measurements

A process flow and instrumentation diagram of the experimental set-up that was used to measure the membrane permeances for single gases is shown in Figure 17. The set-up consists of the membrane module thermostated in an oven, two pressure transducers to measure the pressure at the feed side and at the permeate side of the membrane, a thermocouple that measures the temperature in the membrane and a mass flow controller to measure the flow rate at the permeate side of the membrane.

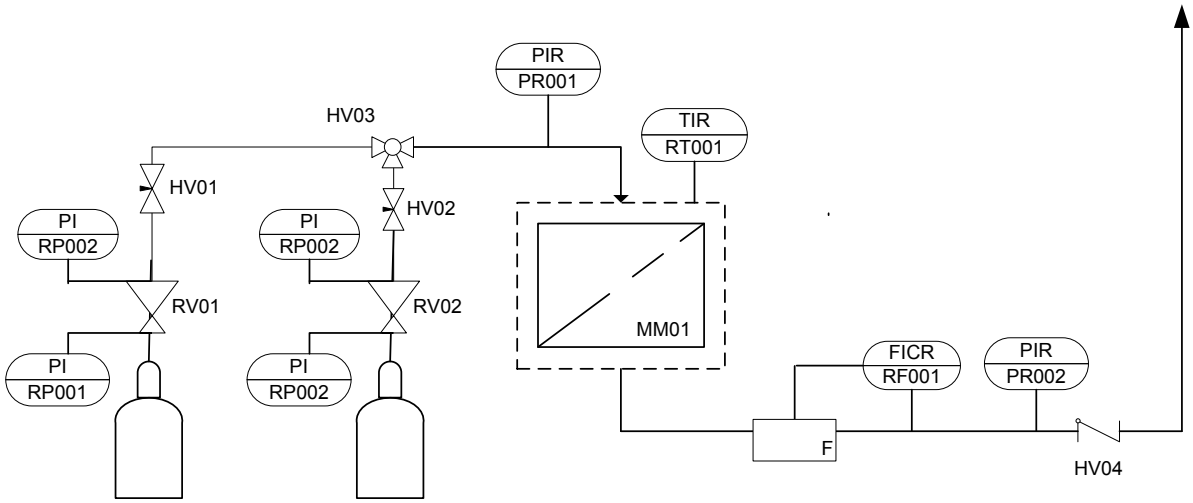

Equipment	Description
PI, PIR	Pressure Indicator, Pressure Indicator Record
TIR, FICR	Temperature Indicator Record, Flow Indicator Control Record
MM, F	Membrane Module, Mass Flow Controller
RV01, RV02; HV01,HV02 HV03; HV04	Pressure Regulator; Needle valve 3-way valve; Check valve

Figure 17 – Process flow and instrumentation diagram of the experimental set-up for single gas permeability measurements.

1.4 Procedure

1.4.1 Commissioning and assembly of the set-up

The first step was commissioning the set-up. The pure gas, helium (Air Liquide, 99,999 % pure) or hydrogen (Air Liquide, 99,999% pure), was supplied to the feed inlet and it flowed across the inside of the membrane to the permeate outlet. The gas pressure on the feed side and on the permeate side of the membranes was measured by two pressure transducers. On the feed side it was used a pressure transducer (MKS instruments model 750B) with a measurement range of 0-5000 mbar and in the permeate side it was also used a pressure transducer (MKS instruments model 750B) with a measurement range of 0-2000 mbar. The two pressure transducers were connected to a controller (MKS Instruments model PR 4000) and the latter was connected to a data acquisition system (YOKOGAWA, model MV100). Since the signal of pressure transducers was in Amperes and the controller signal was in Volt, it was necessary to connect two 50 Ohm resistances to convert the signal of the pressure transducers to Volt. The feed side pressure was controlled by a pressure reducer that connected the system to the gas bottles. The permeate flow rate was measured by a mass flow controller (MKS Instruments model 1179A) that was also connected to the controller and to the data acquisition system. The pressure difference was measured for different flow rates.

The membrane module was thermostated in an oven. For lower temperatures, it was used a closed oven (Heraeus with a temperature range until 250°C) and for temperatures higher than 250°C it was used a cylindrical oven (Heraeus). With the cylindrical oven a controller (Heraeus) was used to control the temperature. In the membrane module the temperature was measured with a thermocouple (type K).

For security reasons, when measuring the membrane permeation for hydrogen, the oven needed to be in inert atmosphere. Therefore, a connection was made between the nitrogen bottle and the oven. The nitrogen flow rate was measured with a rotameter connected to the nitrogen bottle.

Before installing the membrane inside the module the membrane needed to be cleaned. Therefore, the membrane was washed with acetone and dried with air.

After cleaning, the membrane was finally installed in the module. The gas sealing was ensured using graphite rings in between the membrane and the module. After this, the module was assembled in the system. Figure 18 shows a picture of the final set-up using the closed oven, with a description of the equipment and instrumentation.

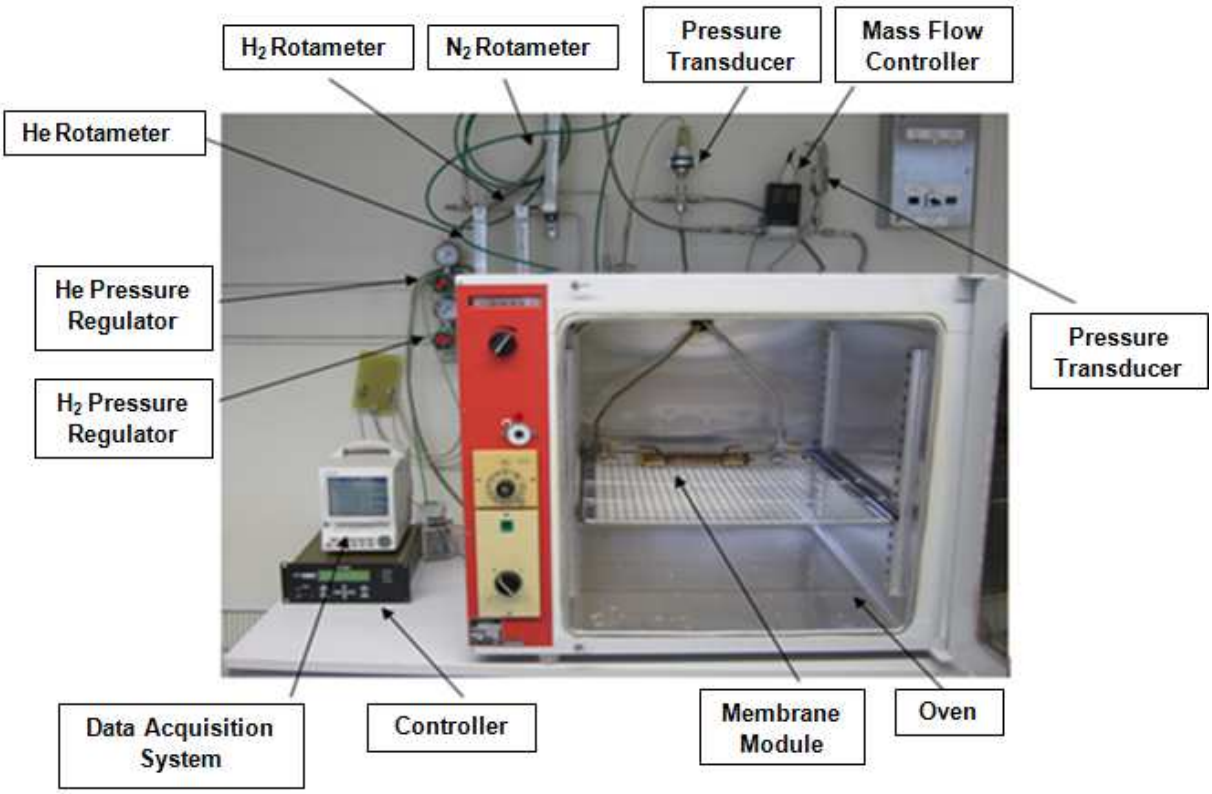

Figure 18 – Final set-up and description of the equipment and instrumentation.

Figure 19 shows a detailed picture of the membrane module inside the oven and corresponding hoses.

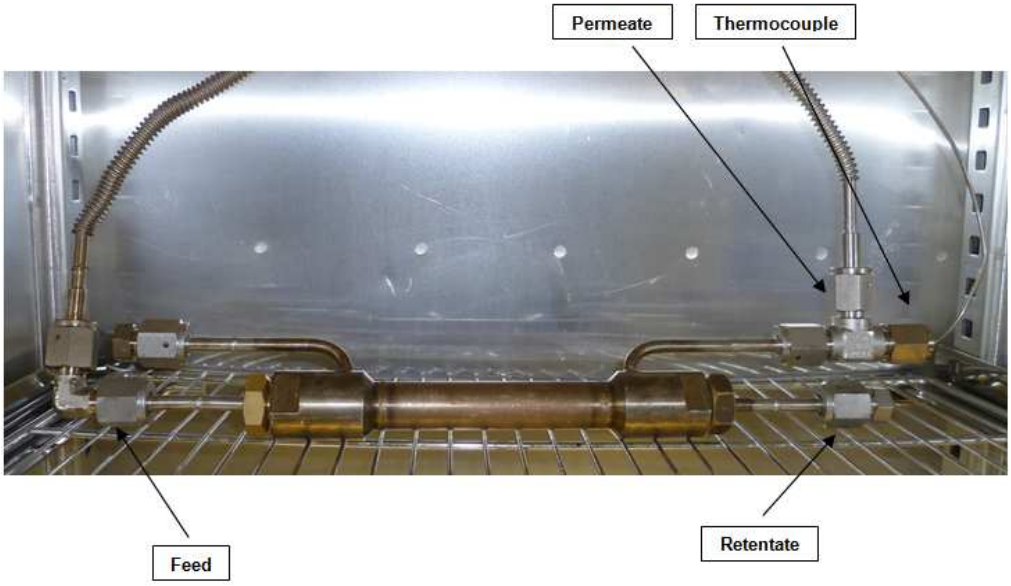

Figure 19 – Detailed picture of the membrane module inside the oven and corresponding hoses.

Figure 20 shows a picture of the cylindrical oven and corresponding temperature controller used throughout the permeation experiments at temperatures higher than 250°C. The edges of the membrane module were covered by fibre glass tape for two reasons: for security reasons because the working temperatures at this oven are extremely high and also to help maintaining a constant temperature inside the oven as its edges are open to the atmosphere.

Figure 20 – Cylindrical oven and corresponding temperature controller.

1.4.2 Leakage tests

After commissioning the set-up and before the permeation experiments an important step is to perform leakage tests in order to check the integrity of the whole set-up.

Technically, a leakage is an unexpected flow due to a hole or porosity that lets the fluid to pass from the higher pressure side to the lower pressure side. Leakage tests were performed to ensure that there was no leakage associated to a hose sealing and they aimed to assure the whole system integrity. In these experiments the method used for leaks detection was to evacuate the system and spray it with helium. Leakage tests with helium are advantageous since helium exists in a very low concentration in the atmosphere, it is non toxic, it is very miscible, relatively cheap and chemically inert. Therefore, it is safe in any environment.

To check the system integrity, before assembling the module, a leakage test was carried out. A vacuum pump (Pfeiffer vacuum, model Turbopumpstand TXV 261) was used to evacuate the system and a leak detector (Pfeifer vacuum Helium leksucher) was connected. This detector consists of a vacuum pump and a mass spectrometer. The hoses were sprayed with helium and when there was a leak the detector showed immediately its value. A leakage test was also performed in the module to check if there were any leaks before connecting it to the system.

After checking the module and the set-up separately, the membrane module was finally assembled to the system and the last leakage test was performed with the leaks detector connected to the mass flow controller outside in order to check the whole set-up integrity.

1.4.3 Mass flow controller calibration

The mass flow controller used in the permeation experiments is calibrated for hydrogen by default. Hence, before it could be used to measure the helium permeate flow rate it was calibrated. For this purpose, it was used a digital flowmeter (Intelligent Digital Flowmeter, Varian analytical instruments) that was connected to the outlet of the mass flow controller. Different flow rates were set in the controller and the different measurements of the mass flow controller and the digital flowmeter were plotted to get a calibration curve. A linear regression was obtained between the helium flow rate measured by the mass flow controller and the helium flow rate measured by the digital flow meter (calibration curve presented in Appendix 1). According to the calibration curve, the helium flow must be multiplied by a factor of 1.5614 to obtain the actual flow rate.

1.4.4 Permeation experiments

The dead-end method was used to measure the membrane permeances for single gases. In this method a pressure difference was applied across the membrane and the stationary permeate flow rate necessary to maintain that pressure difference was measured.

Before starting measuring permeances, the MFI membrane was dried, over night at a temperature of 250°C, by a flow of pure helium in order to remove the adsorbed species, such as water coming from the moisture in the atmosphere. After drying the membrane and before the permeation experiments the set-up was evacuated to set the pressure transducers. For this purpose the vacuum pump was connected to the permeation module and when the system was evacuated, the zero of the pressure transducers was set. Afterwards, the vacuum pump was disconnected and the span of the pressure transducers was set to the atmospheric pressure.

After these procedures, the permeation experiments could finally be carried out. At room temperature, a pressure difference was applied between the feed side and the permeate side of the membrane and the permeate flow was measured. This procedure was repeated for different temperatures ranging from room temperature up to 400°C.

For the permeation experiments of hydrogen, the oven was filled with nitrogen with a flow of 10 L/h during 2 hours when using the closed oven. When using the cylindrical oven a flow of 10 L/h was applied for 10 min before feeding hydrogen to the permeation module. Throughout the experiments a flow of 60 L/h of nitrogen was kept to ensure inert atmosphere inside both ovens.

PART III – RESULTS AND DISCUSSION

1. Results and Discussion

The permeability and selectivity characteristics can widely vary from membrane to membrane due to differences in pore size and defects size and distributions and other structural features such as thickness. These differences result from different supports and synthesis methods, but also for the same type of support, different samples may show differences in permeance and selectivity [19]. Hence, it is essential to determine the permeability and selectivity characteristics of each membrane before its use.

In this work, the temperature dependence of steady-state permeation of a single component through a nanocomposite-MFI zeolite membrane was studied for two different gases, helium and hydrogen, in a wide range of temperatures from room temperature up to 400ºC at a constant pressure difference of 500 mbar. The objective of this work was to study the permeance behaviour of helium and hydrogen as single gases through the nanocomposite-MFI membrane, as well as to identify the optimum operating conditions to obtain high selectivity of hydrogen/helium without jeopardizing the permeance.

.

1.1 Steady State Gas Flow Rate as a Function of the Temperature

The permeance was estimated after the gas flow rate reached steady state over time. Figures 21 and 22 show the time to reach steady state flow rate at different temperatures. Figure 21 shows the time to reach helium steady state flow rate at four different temperatures while figure 22 shows the time to reach hydrogen steady state flow rate for identical temperatures.

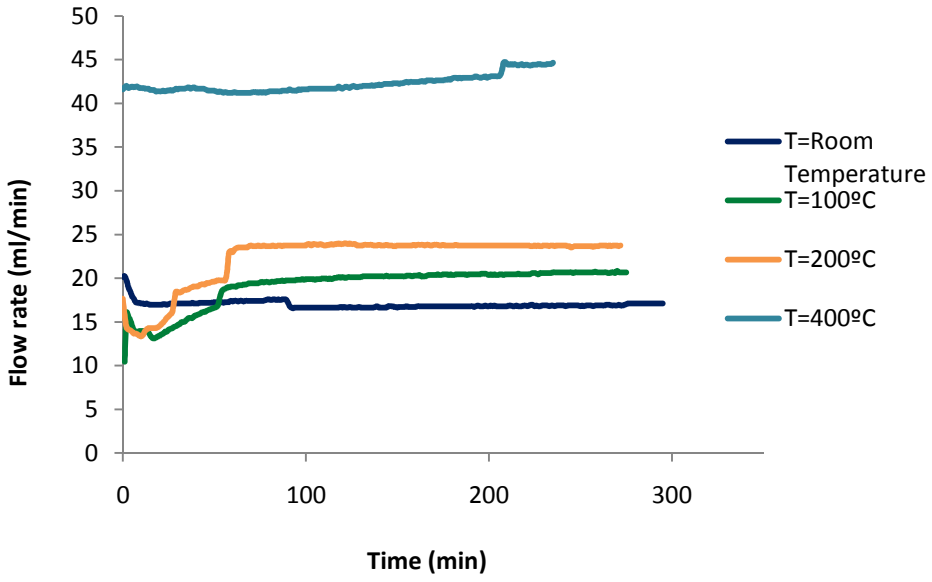

Figure 21 – Time to reach helium steady state flow rate at different temperatures.

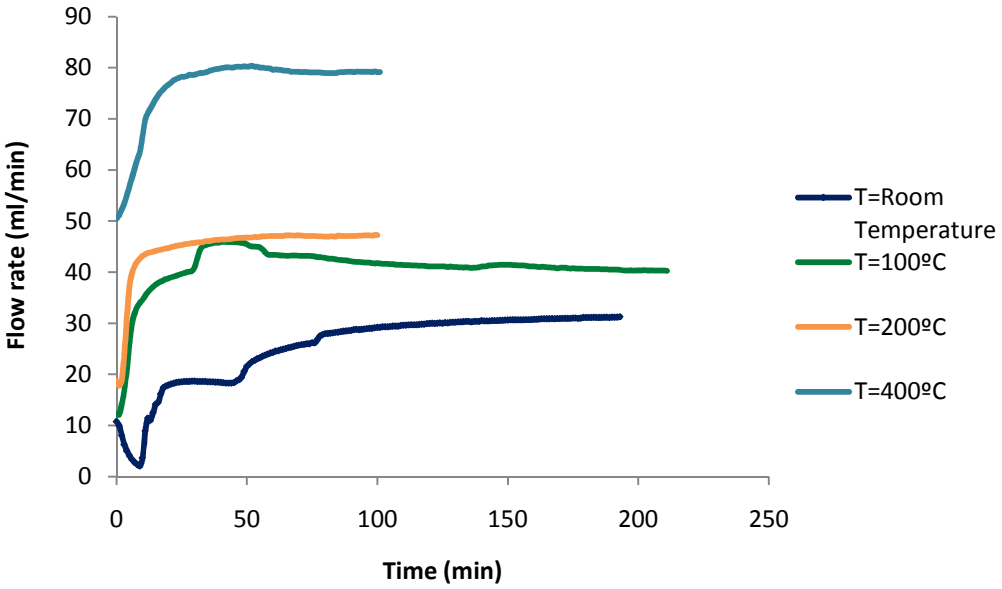

Figure 22 – Time to reach hydrogen steady state flow rate at different temperatures.

Figures 21 and 22 show that for both helium and hydrogen the flow rate follow the same trend over time. In both cases, the average time to reach steady state gas flow rate was between 100 and 200 minutes irrespective of the temperature. The graphs show that the flow rate is temperature dependent increasing significantly with the temperature increase (highest flow rate at 400°C).

The tests aimed to maintain a pressure difference of 500 mbar. However, it was not possible to maintain that pressure difference exactly throughout the experiments, because the permeate side was opened to the atmosphere and there was no valve to maintain it stable. Table 5 summarizes the actual pressure difference maintained and the experimental variation observed in the applied pressure difference for helium and hydrogen.

Table 5 – Summary of pressure differences during the experiments for the two gases.

Gas	Mean pressure difference ± SD (mbar)	Range (mbar)
Hydrogen	507.6 ± 20.6	465 - 557
Helium	507.5 ± 21.1	459 - 540

Figures 23 and 24 show the steady state gas flow rates for helium and hydrogen obtained for each temperature. The respective tables are displayed in Appendix 2, for helium and hydrogen.

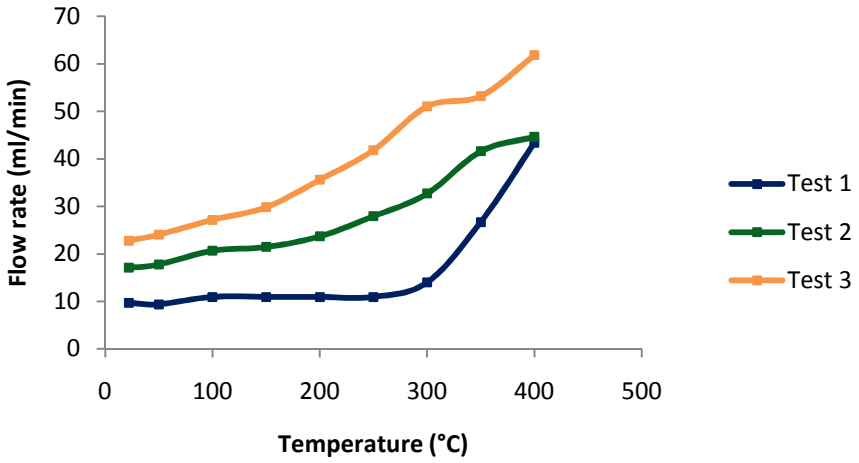

Figure 23 – Helium flow rate at different temperatures.

The helium flow rates observed in the three test runs were significantly different. The helium flow rates observed in the first test were significantly lower than the gas flow rates observed in tests 2 and 3 at temperatures lower than 400°C. However, the results obtained from tests 2 and 3 show similar trends although the actual flow rates were higher at the third test. On average, up to 150°C the steady state helium flow rate did not show a significant increment with increasing temperature. However, beyond 150°C, the gas flow rat significantly increased showing a linear trend (except in test 1).

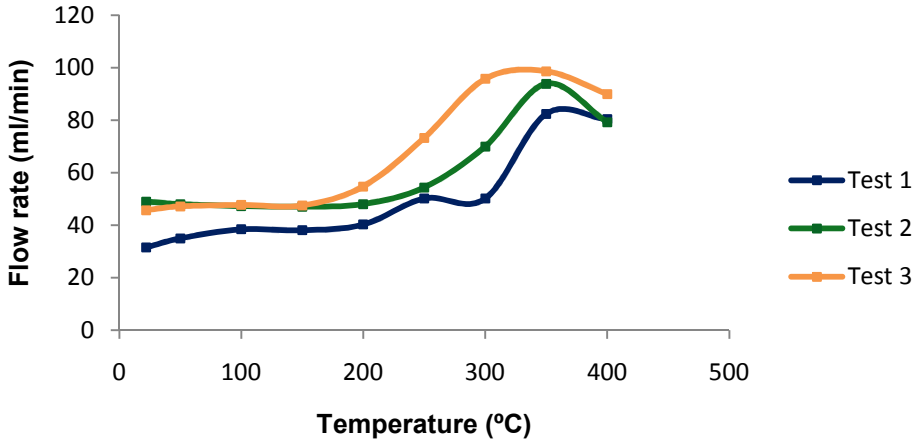

Figure 24 – Hydrogen flow rate at different temperatures.

Unlike the gas flow rates observed for helium the steady state gas flow rates observed for hydrogen in the three test runs presented similar trends. In general, up to 200°C the steady state hydrogen flow rate did not respond to the temperature rise. From 200°C to 370°C the steady state hydrogen flow rate increased with the temperature increase but surprisingly further temperature increase decreased the steady state hydrogen flow rate. The drop in hydrogen flow rate was consistent in all three test runs performed.

1.2 Effect of Temperature on Single Gas Permeance

Wridzer et al., 1997 [20] and Algeri et al, 2003 [21] demonstrated that the permeance of single gases is a function of the temperature and shows different trends at low and high temperatures implying the existence of two different mass-transport mechanisms in the MFI zeolite membranes. *Coronas and Santamaría* (1999) [22] described the permeance based on mass transport mechanisms in microporous membranes (Figure 25). Accordingly, the permeance at low temperatures is governed by by surface diffusion followed by adsorption. The surface diffusion increases with the temperature (AB) whereas adsorption decreases with increasing temperature (BC). The minimum (C) occurs when the amount adsorbed on the membrane vanishes. At higher temperatures the permeance increases again with increasing temperature (CD) due to a different diffusion mechanism which Xiao and Wei, 1992 [23] designated as activated gaseous diffusion or translation diffusion.

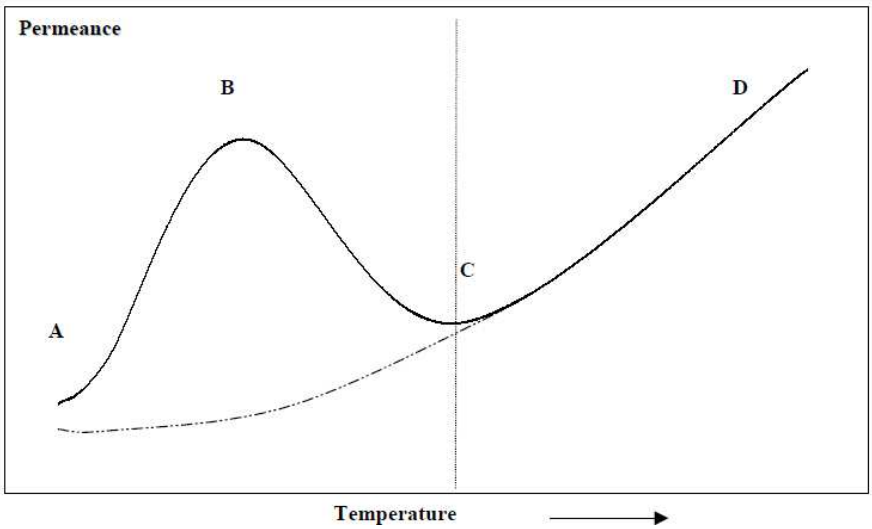

Figure 25 – Typical permeance of a single gas through a zeolite membrane as a function of the temperature[23].

1.2.1 Permeation experiments with single gases

The gas permeance through the membrane for each temperature was calculated using equation (10).

$$P^* = \frac{F(mol/s)}{\Delta P(Pa).A(m^2)} \qquad (10)$$

where, F= gas flow rate, ΔP= pressure difference, A= membrane surface area. The surface area of the membrane was 4.9 x 10^{-4} m^2 [33]. A table with the calculated permeances for helium and hydrogen can be found in Appendix 3 and the expression used to calculate the permeance errors can be found in Appendix 4.

- **Permeation experiments with helium**

Figure 26 shows the experimental permeance for helium at different temperatures for the three tests performed. The trends in permeance follows the trends observed for the gas flow rate (Figure 23). Increasing the temperature from 150ºC up to 400°C resulted in a linear rise in permeance (tests 2 and 3).

In general, the permeance increased by 2.5 fold from room temperature to 400°C. The trend in test 1 was significantly different from the other two tests.

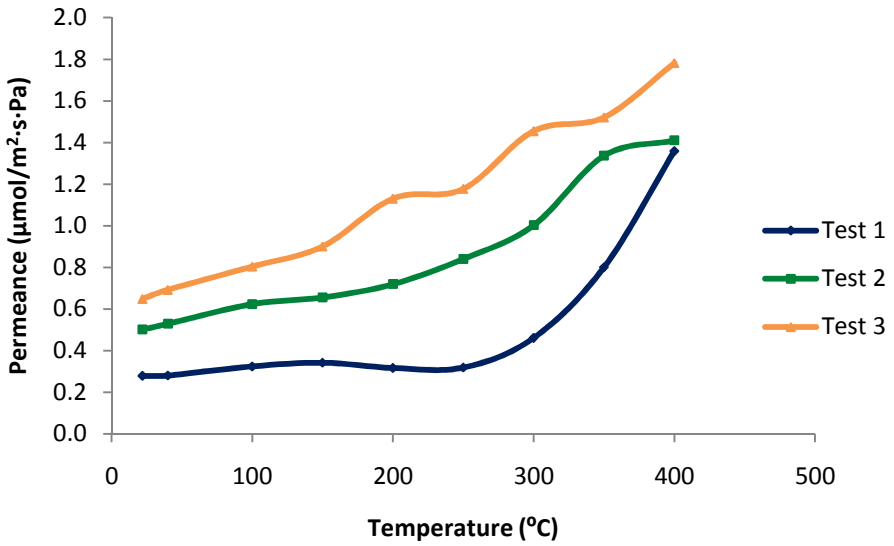

Figure 26 – Permeance of helium at different temperatures.

- **Permeation experiments with Hydrogen**

Figure 27 shows the experimental permeance for hydrogen at different temperatures for the three tests performed. The trends in permeance follows the trends observed for the gas flow rate (Figure 24). Increasing the temperature up to 200°C resulted in a constant permeance; increasing the temperature from 200 up to 370°C showed a linear rise of the permeance and from 370°C onward a decreasing in hydrogen permeance was observed.

In general, the permeance increased by 1.2 fold from room temperature to 370°C. The permeance decreased by about 7% in the range 370ºC – 400ºC. Due to the membrane stability, these experiments did not extend beyond 400°C, hence no data are available to investigate the observed trend beyond 400°C.

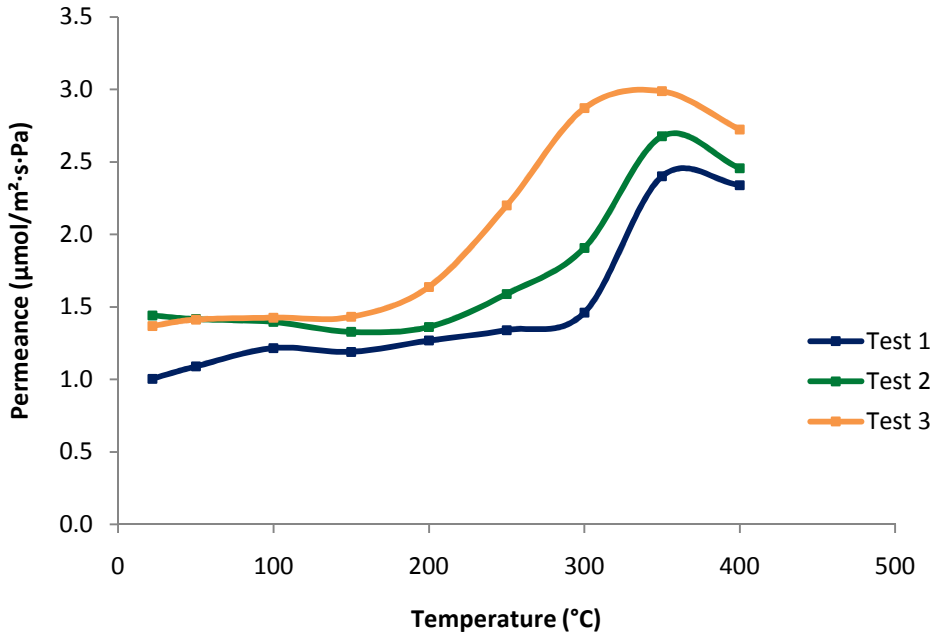

Figure 27 – Permeance of hydrogen at different temperatures.

1.3 Single Gas Transport Mechanisms in the Nanocomposite-MFI Membrane

1.3.1 Helium permeance

A rising trend in helium permeance was observed with increasing temperature for the three tests performed as shown in Figure 26. The permeance trends observed for helium are not in line with the behaviour expected for MFI zeolite membranes with single gases as described in 1.2. Helium being a noble gas has no affinity towards MFI Zeolite and it is reported that its adsorption on MFI zeolite is null [20]. Hence, adsorption mechanism is not applicable to helium. The transport of helium through the MFI zeolite membrane can be attributed to an activated gaseous diffusion process (CD in Figure 25) and the permeance is controlled by the helium mobility in the zeolite pores.

Kanezashi and Lin (2009) [24] explained the permeance of non-adsorbing or weakly adsorbing small gas molecules, such as helium and hydrogen through MFI zeolite membranes by a modified Fick´s equation (11) that takes into account the physical properties of the gas and of the MFI zeolite membrane to describe permeance:

$$P = \frac{\varphi \alpha \beta}{Lz}\left(\frac{8RT}{\pi M}\right)^{1/2} \exp\left(-\frac{E_d}{RT}\right) \qquad (11)$$

where P is the Permeance, E_d is the activation energy for gas diffusion, M is the molecular weight, φ is the ratio of the membrane porosity to the tortuosity factor, β is a constant of the gas molecule, L is the membrane thickness, R is the gas constant, T is the temperature, α is the diffusion length

(distance between two adjacent sites) and z is the diffusion coordination number. This model data and results, for non-adsorbing molecules, is described in Appendix 5 for helium and for hydrogen permeances.

The estimated permeance using activated diffusion equation for temperatures between room temperature and 500°C is shown in Figure 28:

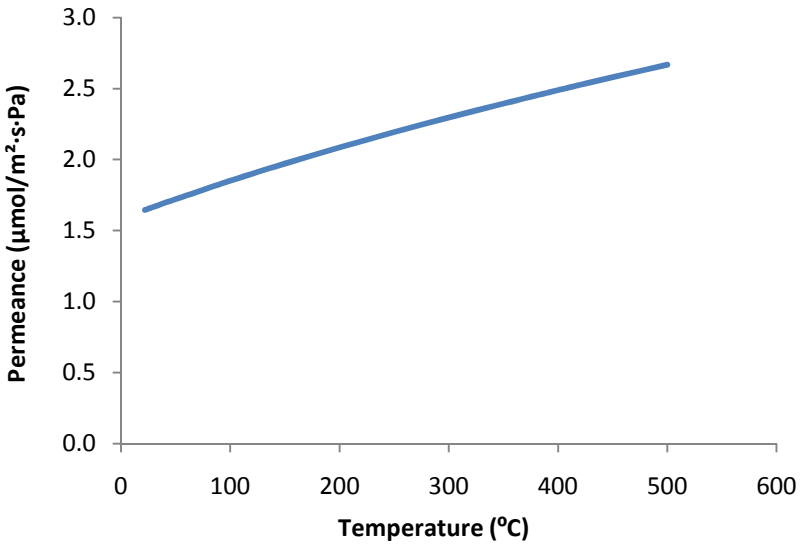

Figure 28 – Estimated permeance for Helium as a funtion of the temperature using The Modified Fick´s diffusion equation.

The linear trend derived using the modified Fick´s diffusion equation can explain the permeance observed experimentally. Thus, helium permeance occured only by activated gaseous diffusion, since the permeance continuously increased with temperature, as theoretically predicted for non-adsorbing molecules

Although the three tests performed with helium showed the same trend of permeance with the temperature, the first test data were different from the second and third tests data. Most likely, this was due to moisture that was initially condensed in the membrane. The temperature used to dry the membrane was 250°C. Further experiments revealed that this temperature was not high enough to dry all the adsorbed water from the air in the membrane. Therefore, in the first test there was moisture blocking the membrane pores which limited the helium flow. In the first test, the helium permeance was low and did not increase significantly until 300°C. Further increase in the temperature helped to remove the remaining moisture and the helium permeance increased linearly with increasing temperature. In the second and third tests since the membrane had been previously heated up to 400°C this behaviour was not observed and the helium permeance showed a linear increase with the temperature.

1.3.2 Hydrogen permeance

A constant trend in hydrogen permeance was observed with increasing temperature until 200°C and from 200ºC onwards it was observed a linear increase with a maximum permeance at 370°C. The same behaviour was observed in the three tests performed. The behaviour observed does not comply with the general behaviour explained by Xiao and Wei, 1992 [23] for MFI zeolite membranes (Figure 25). Hydrogen is an inorganic molecule weakly adsorbed on MFI membranes [25]. Therefore, adsorption-surface diffusion was expected to be weak for hydrogen.

The same model used for helium was applied to hydrogen to predict the theoretical behaviour of hydrogen permeance with the temperature. The estimated permeance for temperatures between room temperature and 500ºC is shown in Figure 29:

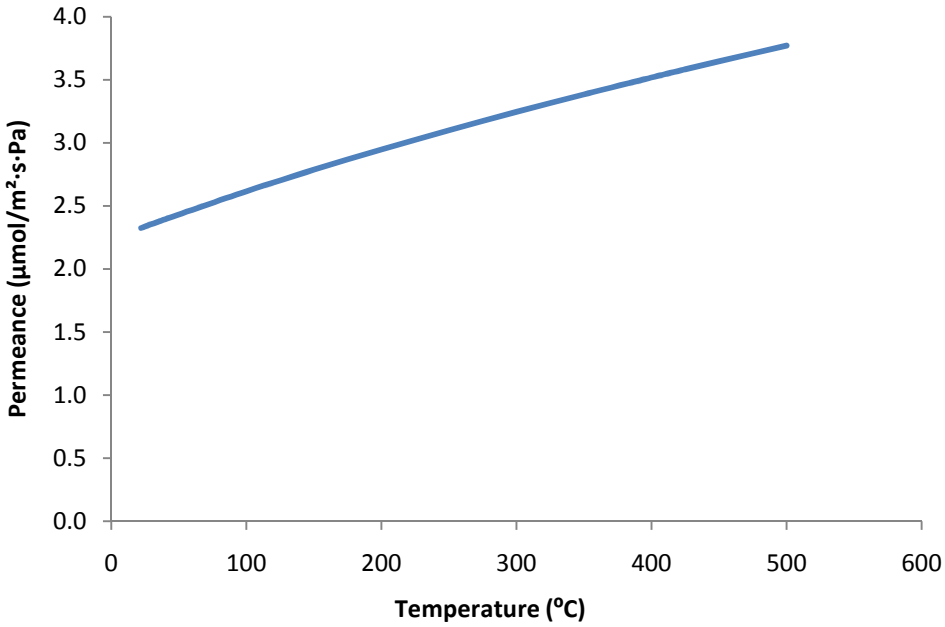

Figure 29 – Estimated permeance for hydrogen as a funtion of the temperature using modified Fick´s diffusion equation.

The linear rising trend derived using the modified Fick´s diffusion equation can somewhat explain the hydrogen permeance observed experimentally. However, the constant permeance observed from room temperature to 200ºC and the decrease in hydrogen permeance beyond 370ºC was not predicted by this model. The constant permeance until 200ºC can be explained by the fact that hydrogen is weakly adsorbed leading to slow permeance at low temperatures via adsorption mechanisms. This mechanism ceased at 200ºC and the permeance from then on was controlled by activated gaseous diffusion. The decrease observed beyond 370ºC could be due to physical interactions of the hydrogen molecules with the membrane material.

1.3.3 Comparison of helium and hydrogen permeances

Figure 30 shows a comparison of the average permeances of Helium (average of tests 2 and 3) and Hydrogen at different temperatures. Hydrogen permeance is on average 1.3 fold higher than Helium permeance and the gap between them was higher at high temperatures. This permeance gap between helium and hydrogen is fundamental for a good separation of the two gases.

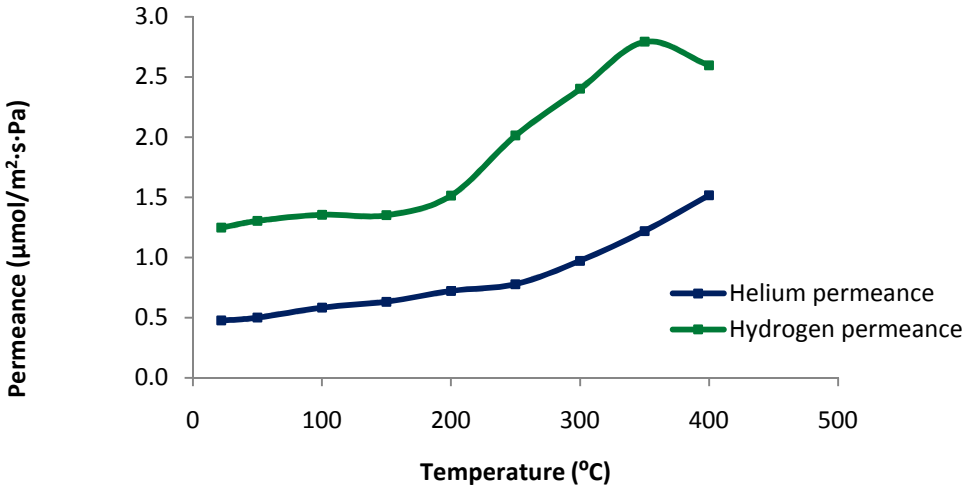

Figure 30 – Comparison of helium and hydrogen permeances at different temperatures.

1.4 Hydrogen/Helium Ideal Selectivity

The ideal selectivity is an indicator to assess the membrane separation performance, and this parameter is only based on single gas permeance measurements. The ideal selectivity and the real selectivity may differ because the experimental permeances of single gases do not always involve the effects of individual components in a gas mixture on the permeation.

The hydrogen/helium ideal selectivity was determined by the ratio of hydrogen and helium permeances according to equation (9). Figure 31 shows the behaviour of hydrogen/helium ideal selectivity with the temperature for the three tests performed. The graph shows two maxima. At first, the selectivity decreased up to 150°C and then it increased from 150°C to 300°C. The ideal selectivity decreased again from 300°C onwards. The high ideal selectivities observed for the test 1 should not be considered due to moisture condensation inside the membrane pores that led to low gas permeance.

Due to the close kinetic diameter of both molecules (0.26 and 0.29 nm, respectively for He and H_2) and since both molecules are considerably smaller than the pore size of the MFI zeolite membrane (0.55 nm) molecular sieving is not expected to play any role in the separation process. Therefore, it

can be assumed that helium and hydrogen were separated due to hydrogen higher permeance in the temperature range studied.

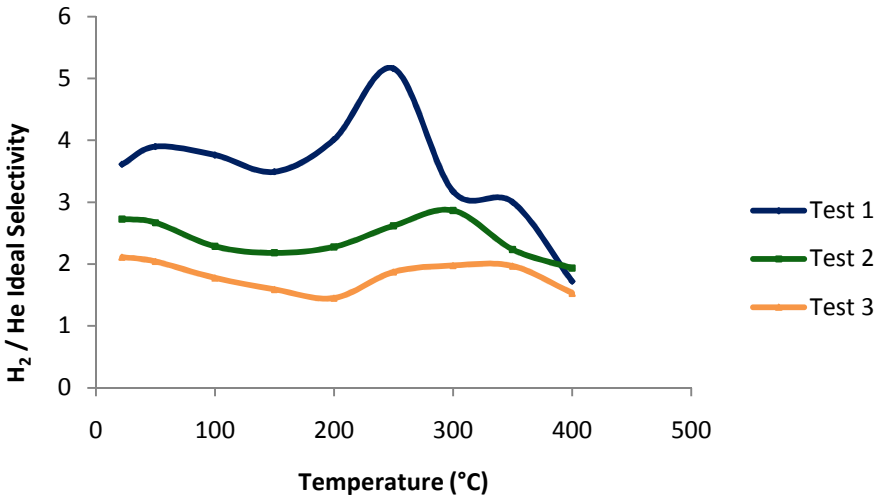

Figure 31 – Hydrogen / Helium ideal selectivity at different temperatures.

Figure 32 shows the average permeances of helium and hydrogen, as well as the average of hydrogen/helium ideal selectivity as a function of the temperature. The graph shows that the average ideal selectivity is higher at room temperature and at 300°C. In order to obtain a high membrane performance two factors should be taken into account; (1) the membrane must have a high selectivity but also (2) the membrane permeance should be high. Based on the selectivity estimated it can be concluded that the best operating temperature for maximum helium/hydrogen selectivity is 300°C (Figure 32).

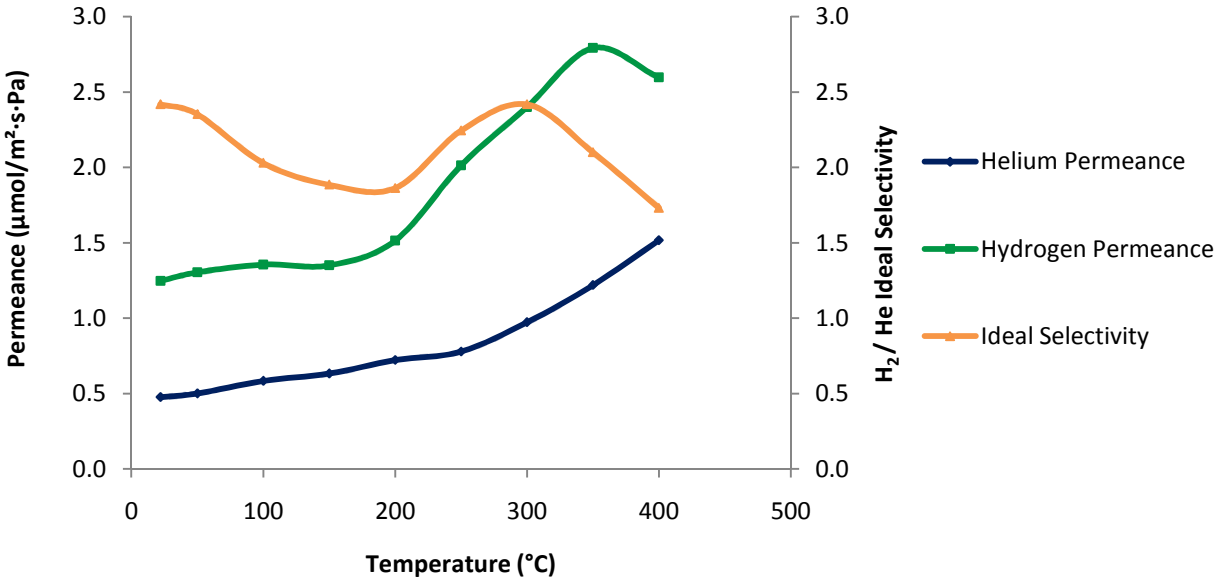

Figure 32 - Ideal selectivity average and permeances average for helium and hydrogen.

1.5 Defects in Microporous Membranes

According to Koutsonikolas et al. [27], for single gas permeation in microporous media, the gas transport through the defects (2 nm <d_p < 50 nm) can be described by Knudsen diffusion. Equation (12) represents the Knudsen permeance for a single gas [28].

$$P_{kn} = \frac{2\varepsilon\ r_p}{3\tau\ L}\left(\frac{8}{\pi RTM}\right)^{1/2} \tag{12}$$

where, ε is the porosity (0.075) [26], r_p is the pore radius (0,55 nm) [26], τ is the tortuosity (1.2)[26], L the thickness of the membrane (1 μm) [26], R is the gas constant, T is the temperature and M is the molecular weight of the gas.

The Knudsen selectivity is also an indicator of the presence of defects in the microporous membrane, and it can be calculated using equation (13) [28]:

$$\alpha_{kn} = \sqrt{\frac{M_{He}}{M_{H_2}}} \tag{13}$$

where M is the molecular weight.

Whether a membrane contains defects, the gases transport through the defects gives rise to an increase in the gases permeances and a decrease in the selectivity.

Figure 33 shows the theoretical Knudsen permeance with temperature for helium and hydrogen using equation (12). A table containing the data calculated for both gases is displayed in Appendix 6. According to the graph, the Knudsen diffusion mechanism would lead to the permeance decrease with increasing temperature.

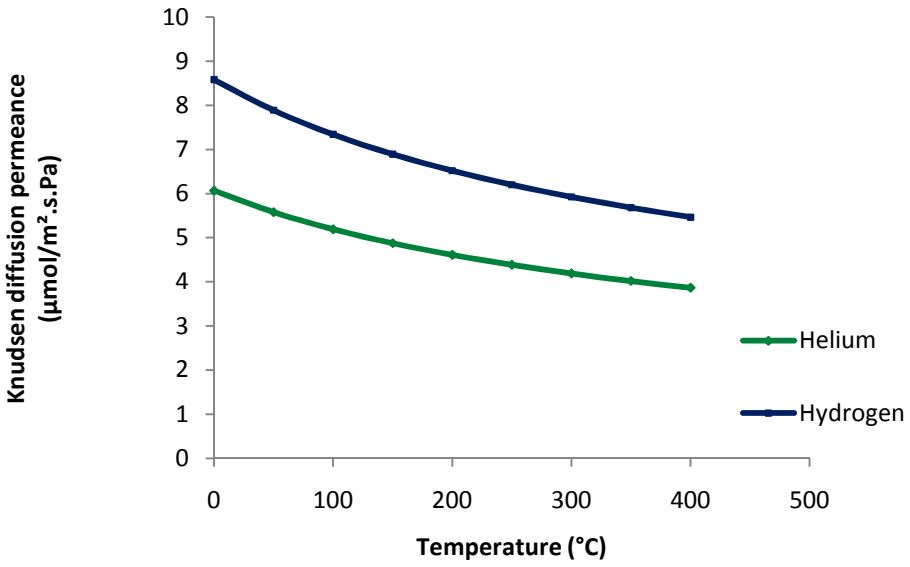

Figure 33 – Knudsen diffusion permeance for helium and hydrogen calculated by equation (12).

Comparing the experimental permeances obtained in this study with the theoretical Knudsen permeances, it was possible to conclude that the permeances of helium and hydrogen in the nanocomposite-MFI membrane were not governed by a Knudsen diffusion mechanism since the experimental permeances of both gases increased with increasing temperature. Moreover, the experimental permeances obtained in this study were slightly lower than the theoretical Knudsen permeances. This observation associated with the fact that the ideal selectivity obtained was higher than the Knudsen selectivity (α_{kn} = 1,4) indicated that the membrane did not contain large defects, thus the flow was mainly through the micropores.

Although no large defects were identified, the permeances of helium and hydrogen (Figures 26 and 27) increased from test 1 to test 3 in both cases. This fact reveals that there was a small leakage in the module, probably due to graphite seals loose tightness or due to small defects in the membrane the size of which increased with the temperature, which in turn led to increasing single gas permeances and decreasing H_2/He ideal selectivity.

1.6 Comparison with Literature Data

Single gas permeation through zeolite membranes have been reported in the literature for different types of zeolite membranes. Table 6 makes a comparison between the results of this work and the data obtained with other zeolite membranes. Results are compared for the non-adsorbed helium and the weakly adsorbed hydrogen, as well as for the hydrogen/helium ideal selectivity.

Table 6 – Comparison of reported single gas permeation data through different non-commercial zeolites membranes.

Membrane	**Temperature (ºC)**	**Permeance (µmol/m².s.Pa)**		**H_2/He Ideal selectivity**	**Reference**
		Helium	**Hydrogen**		
Silicalite-1	25	8,8	22,3	2,5	[29]
Microporous titanosilicate AM-3 membrane	25	0,07	0,1	1,7	[30]
Silicalite-1	25	8,3	21,5	2,6	[31]
ZSM-5		5,8	15,7	2,7	
Alumina/Silica zeolite	100	0,2	0,2	1,3	[32]
Alumina/Silica zeolite modified with SiO_2		0,04	0,09	2,3	
Nanocomposite-MFI	25	0,5	1,3	2,6	Current work
	100	0,6	1,4	2,3	
	300	0,9	2,4	2,5	

Differences in the permeation through different membrane types have been reported in the literature. For the membranes displayed in Table 6 the ideal selectivity was quite similar (1,3 – 2,7) regardless the temperature. As for the permeances of helium and hydrogen, through the nanocomposite-MFI membrane, 0,5 – 0,9 µmol/m².s.Pa and 1,3 – 2,4 µmol/m².s.Pa, respectively, they were among the range of the other membranes permeances, for helium 0,04-8,8 µmol/m².s.Pa and for hydrogen 0,09 – 22,3 µmol/m².s.Pa.

1.7 Stability of the Membrane with Temperature and Operation Time

The long-term durability of the membranes and their thermal and chemical stabilities are key issues in the selection of a membrane for a certain process. The third permeation test for helium, carried out for about 300 h of operation, 20 h of which at 400ºC, showed that the membrane kept its integrity. As there was a small leak in the module, most likely more tests are needed to check the membrane performance. The results presented in this thesis are a preliminary indicator of the thermal and mechanical stability of the membrane.

CONCLUSIONS AND FUTURE PERSPECTIVES

Conclusions

This thesis aimed to assess the potential use of zeolite membranes for tritium processes. There is a lack of experimental data on permeation and selectivity of helium and hydrogen through zeolite membranes and this study attempted to bridge that gap. In order to achieve this purpose, the first step consisted in commissioning the set-up for single gases experiments and the second step comprised the permeation experiments of helium and hydrogen through a nanocomposite-MFI membrane. Single gas permeances were measured for different temperatures and the corresponding ideal selectivity was determined.

The first part of the work was successfully accomplished and an apparatus was assembled. The set-up can now be up-graded for permeation tests of gas mixtures and water steam.

The second part of the work allowed to conclude that the nanocomposite-MFI membrane shows hydrogen/helium selectivity, thus this membrane may be used to separate these two gases. Moreover, this membrane can be used at high temperatures yielding simultaneously high permeances and selectivity.

The membrane was operated for approximately 300 h, 20 of which at 400°C, showing that the membrane is mechanically strong and thermally and chemically stable. Two important problems have been highlighted and solved: the membranes must be dried at 400ºC to evaporate the residual water inside the pores and the membrane module should be duly sealed in order to obtain reliable results.

A general conclusion that can be drawn from this work is that the nanocomposite-MFI membrane seems appropriate to the pre-separation and the pre-concentration step of the Tritium Extraction System in the breeder blanket of the future fusion machines.

Future Perspectives

The work carried out provided insight into the characteristics of nanocomposite-MFI membrane. However, more experimental data are needed: single gases, gas mixtures, water steam and tritium. A model for cascade simulation is also necessary to proceed with the study. Additionally, permeation tests with other membrane materials would be useful in order to compare and select the most suitable material for the pre-separation and the pre-concentration process in the breeder blanket.

REFERENCES

References

1. http://www.iter.org/sci/whatisfusion (November 2010);

2. http://fusionforenergy.europa.eu/ (November 2010);

3. http://www.thefullwiki.org/nuclear_fusion (November 2010);

4. http://www.efda.org/fusion_energy/ (November 2010);

5. http://www.jet.efda.org/ (January 2011);

6. http://www.worldenergy.org/ (January 2011);

7. D. Demange, *Selective permeation for breeder blanket at the Tritium Laboratory Karlsruhe* 2010, Karlsruhe Institute of Technology (personal presentation);

8. D. Demange, S. Stämmler., M. Kind, *A new combination of membranes and membrane reactors for improved tritium management in breeder blanket of fusion machines, 26th SOFT, September 2010, Porto, Portugal*;

9. F. Cismondi, *Basics of breeding blanket technology*, 2010, Karlsruhe Intitute of Technology: Karlsruhe (personal presentation);

10. http://www.luvitec.com/ (December 2010).

11. F. Schüth, K.W. Sing, J. Weitkamp, *Handbook of Porous Solids,* Wiley-VCH, 2002;

12. R. Abedini, A. Nezhadmoghadam, *Application of membrane in gas separation processes: its suitability and mechanism,* Petroleum Coal, **52**, (2010), p. 69-80.

13. K. Scott, R. Hughes, *Industrial Membrane Separation Technology*, 1st ed, Blackie Academic & Professional, Glasgow, 1996;

14. R. Noble, S. Stern, *Membrane separations Technology Principles and Applications*, Elsevier, Amsterdan, 1995;

15. M. Pera-Titus, *Preparation, characterization and modeling of zeolite NaA membranes for the pervaporation dehydration of alcohol mixtures*, Doctoral Thesis, Chemical Engineering Department, University of Barcelona, 2006;

16. http://materials.binghamton.edu/labs/zeolite/zeolite.html (March 2011);

17. S. Miachon, E. Landrivon, M. Aouine, Y. Sun, I. Kumakiri, Y. Li, O. Prokopová, N. Guilhaume, A. Giroir-Fendler, H. Mozzanega, J. Dalmon, *Nanocomposite MFI-alumina membranes via pore-plugging synthesis Preparation and morphological characterization,* Journal of Membrane Science, **281** (2006), p. 228-238;

18. Y. Li, M. Pera-Titus, G. Xiong, W. Yang, E. Landrivon, S. Miachon, J. Daimon, *Nanocomposite MFI-alumina membranes via pore-plugging synthesis: Genesis of the zeolite material,* Journal of Membrane Science, **325** (2008), p. 973-981;

19. Y. Yampolskii, I. Pinnau, B. Freeman, *Materials science of membranes for gas and vapor separation,* John Wiley & Sons, Ltd, Texas, 2007;

20. W. Bakker, L. van den Broeke., F. Kapteijn, J. Moulijn, *Temperature dependence of one-component permeation through a silicalite-1 membrane,* AIChE, **43**(9) (1997) p. 2203-2214;

21. C. Algieri, P. Bernardo, G. Golemmea, G. Barbieria, E. Driolia, *Permeation properties of a thin silicalite-1 (MFI) membrane,* Journal of Membrane Science, **222**(1-2) (2003) p. 181-190;

22. J. Coronas, J. Santamaría, *Separations Using Zeolite Membranes,* Separation & Purification Reviews, **28**(2) (1999) p. 127-177;

23. J. Xiao, J. Wei, *Diffusion mechanism of hydrocarbons in zeolites,* Chemical Engineering Science, **47**(5) (1992) p. 1123-1141;

24. M. Kanezashi, Y. S. Lin., *Gas Permeation and Diffusion Characteristics of MFI-Type Zeolite Membranes at High Temperatures,* The Journal of Physical Chemistry C, **113**(9) (2009) p. 3767-3774;

25. X. Zhu, H. Wang, Y. Lin, *Effect of the Membrane Quality on Gas Permeation and Chemical Vapor Deposition Modification of MFI-Type Zeolite Membranes,* Industrial and Engineering Chemistry Research, **49**(20) (2010) p. 10026-10033;

26. S. Miachon, P. Ciavarella, L. van Dyk, I. Kumakiri, K. Fiaty, Y. Schuurman, J. Dalmon, *Nanocomposite MFI-alumina membranes via pore-plugging synthesis: Specific transport and separation properties,* Journal of Membrane Science, **298**(1-2) (2007) p. 71-79;

27. D. Koutsonikolas, S. Kaldis, G. Sakellaropoulos, M. Loon, R. Dirrix, R. Terpstra, *Defects in microporous silica membranes: Analysis and repair,* Separation and Purification Technology, **73**(1) (2010) p. 20-24;

28. R. Xu, J. Chen, Z. Gao, W. Yan, *From Zeolites to Porous MOF Materials - the 40th Anniversary of International Zeolite Conference* in *Proceedings of the 15th International Zeolite Conference*, Elsevier, Beijing, P. R. China, 2007;

29. S. Wirawan, *Single Gas Permeation through a Modified Silicalite-1 Membrane,* ASEAN Journal of Chemical Engineering, **10**(1) (2010) p. 35 – 44;

30. P. Lito, C. Zhou, A. Santiago, A. Rodrigues, J. Rocha, Z. Lin, C. Silva, *Modelling gas permeation through new microporous titanosilicate AM-3 membranes,* Chemical Engineering Journal, **165**(2) (2010) p. 395-404;

31. S. Rezai, J. Lindmark, C. Andersson, F. Jareman, K. Möller, J. Hedlund, *Water/hydrogen/hexane multicomponent selectivity of thin MFI membranes with different Si/Al ratios,* Microporous and Mesoporous Materials **108**(1-3) (2008) p. 136-142;

32. S. Nitodas, E. Fawas, G. Romanos, M. Papadopoulou, A. Mitropoulos, N. Kanellopoulos, *Development and characterization of silica-based membranes for hydrogen separation,* Journal of Porous Materials **15**(5) (2007) p. 551-557;

33. M.O. Daramola, A.J. Burger, M. Pera-Titus, A. Giroir-Fendler, S. Miachon, L. Lorenzen, J.-A. Dalmon, *Nanocomposite MFI–ceramic hollow fibre membranes via pore-plugging synthesis: Prospects for xylene isomer separation,* Journal of Membrane Science, 337 (2009) p.106-111.

APPENDIX

Appendix 1: Mass flow controller calibration curve

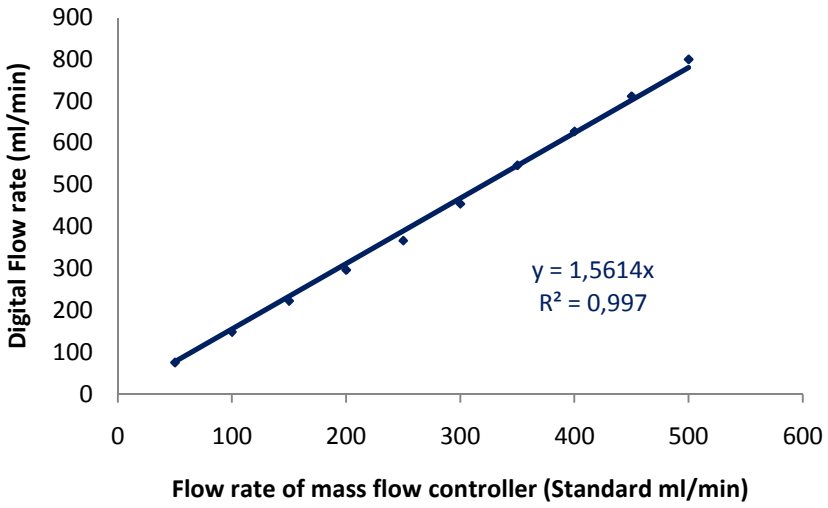

Figure 34 – Mass Flow Controller calibration curve for helium.

Appendix 2: Flow rates of helium and hydrogen at steady state

Table 7 – Helium gas flow rate at steady sate.

Pressure difference	Temperature (°C)	Flow rate (ml/min)		
		First test	Second test	Third test
ΔP = 507 ±21 mbar Min=459 mbar Max=540 mbar	Room	9,7	17,1	22,8
	40	9,4	17,8	24,1
	100	10,9	20,7	27,2
	150	10,9	21,5	29,8
	200	10,9	23,7	35,6
	250	10,9	27,9	41,8
	300	14,0	32,7	51,1
	350	26,7	41,6	53,2
	400	43,4	44,7	61,8

Table 8 – Hydrogen gas flow rate at steady state.

Pressure difference	Temperature (°C)	Flow (ml/min)		
		First test	Second test	Third test
ΔP = 507 ±20 mbar Min=465 mbar Max=557 mbar	Room	31,5	48,9	45,7
	40	35,0	48,0	47,2
	100	38,5	47,3	47,7
	150	38,1	47,0	47,5
	200	40,3	48,0	54,7
	250	50,2	54,4	73,2
	300	50,2	69,9	95,7
	350	82,4	93,9	98,6
	400	80,4	79,2	89,9

Appendix 3: Helium and Hydrogen permeances for different temperatures

Table 9 – Experimental conditions and results obtained for helium permeance.

Pressure difference	Temperature (°C)	Permeance (μmol/m²·s·Pa)		
		Test 1	Test 2	Test 3
ΔP = 507 ±21 mbar Min=459 mbar Max=540 mbar	Room	0.28 ± 0.16	0.50 ± 0.16	0.65 ± 0.18
	40	0.28 ± 0.15	0.53 ± 0.16	0.69 ± 0.16
	100	0.32 ± 0.15	0.62 ± 0.17	0.80 ± 0.17
	150	0.34 ± 0.16	0.66 ± 0.17	0.90 ± 0.18
	200	0.32 ± 0.15	0.72 ± 0.17	1.13 ± 0.20
	250	0.32 ± 0.15	0.84 ± 0.18	1.18 ± 0.25
	300	0.46 ± 0.17	1.00 ± 0.19	1.45 ± 0.20
	350	0.80 ± 0.25	1.34 ± 0.22	1.52 ± 0.21
	400	1,14 ± 0.22	1.41 ± 0.23	1.78 ± 0.23

Table 10 – Experimental conditions and results obtained for hydrogen permeance.

Pressure difference	Temperature (°C)	Permeance (µmol/m²·s·Pa)		
		Test 1	Test 2	Test 3
ΔP = 507 ±21 mbar Min=465 mbar Max=557 mbar	Room	1.00 ± 0.20	1.44 ± 0.21	1.37 ± 0.21
	40	1.09 ± 0.20	1.42 ± 0.15	1.41 ± 0.21
	100	1.22 ± 0.21	1.40 ± 0.21	1.43 ± 0.21
	150	1.19 ± 0.20	1.33 ± 0.16	1.43 ± 0.21
	200	1.27 ± 0.21	1.36 ± 0.20	1.64 ± 0.23
	250	1.64 ± 0.25	1.59 ± 0.22	2.20 ± 0.28
	300	1.46 ± 0.21	1.91 ± 0.23	2.87 ± 0.34
	350	2.40 ± 0.29	2.68 ± 0.31	2.99 ± 0.36
	400	2.34 ± 0.28	2.46 ± 0.31	2.72 ± 0.33

Appendix 4: Permeance error

The permeance error was calculated using the following expression:

$$\left(\frac{\Delta P}{P}\right)^2 = \left(\frac{\Delta F}{F}\right)^2 + \left(\frac{\Delta(\Delta P)}{\Delta P}\right)^2$$

where *ΔP* is the permeance error, *ΔF* is the error of the mass flow controller (5 ml/min) e *Δ (ΔP)* is the error of the pressure difference that was calculated using the following expression:

$$(\Delta(\Delta P))^2 = (\Delta P_{feed})^2 + (\Delta P_{permeate})^2$$

where ΔP_{feed} is the error of the pressure transducer on the feed side (50 mbar) and $\Delta P_{permeate}$ is the error of the pressure transducer on the permeate side of the membrane (20 mbar).

Appendix 5: Theoretical model for activated diffusion

The activated diffusion of non-adsorbing or weakly adsorbing molecules in an MFI membrane is described by the following equation:

$$P = \frac{\varphi \alpha \beta}{Lz}\left(\frac{8RT}{\pi M}\right)^{1/2} \exp\left(-\frac{E_d}{RT}\right)$$

where

P – Permeance (mol/m^2.s.Pa)

Ed – Activation energy for gas diffusion in the micropores (E_{dHe}=7.1 kJ/mol; E_{dH_2}=10.2 kJ/mol) [25]

M – Molecular weight of the gas

φ - Ratio of the membrane porosity to the tortuosity factor (0,075/1,2) [25]

β - Constant of the gas molecule load in zeolite (β =1/RT for diffusion of small molecules)

L- Membrane thickness (1 μm) [33]

R - Gas constant

α - Diffusion length (distance between two adjacent sites) - 1 nm for diffusion in MFI-type zeolite

z – Diffusion coordination number (4 for MFI-type zeolite)

T - Temperature

Table 11 shows the parameters of the theoretical model calculated for helium whereas table 12 shows the parameters calculated for hydrogen.

Table 11 – Parameters of the theoretical model calculated for helium.

Temp (K)	Temp (ºC)	β x10^4 (mol/kJ)	$\left(\frac{8RT}{\pi M}\right)^{1/2}$	$\exp\left(-\frac{E_d}{RT}\right)$	P (μmol/m^2·s·Pa)
295	22	4,08	39,51	0,997	1,65
313	40	3,84	40,70	0,997	1,70
373	100	3,22	44,43	0,998	1,85
423	150	2,84	47,32	0,998	1,97
473	200	2,54	50,04	0,998	2,09
523	250	2,30	52,61	0,998	2,19
573	300	2,10	55,07	0,999	2,30
623	350	1,93	57,42	0,999	2,39
673	400	1,79	59,68	0,999	2,49
698	425	1,72	60,78	0,999	2,54
723	450	1,66	61,86	0,999	2,58
748	475	1,61	62,92	0,999	2,62
773	500	1,56	63,96	0,999	2,67

Table 12 – Parameters of the theoretical model calculated for hydrogen.

Temp (K)	Temp (ºC)	β x10^4 [mol/kJ]	$\left(\frac{8RT}{\pi M}\right)^{1/2}$	$\exp\left(-\frac{E_d}{RT}\right)$	P (µmol/m^2.s.Pa)
295	22	4,08	55,88	0,996	2,32
313	40	3,84	57,56	0,996	2,39
373	100	3,22	62,84	0,997	2,62
423	150	2,84	66,92	0,997	2,79
473	200	2,54	70,76	0,997	2,95
523	250	2,30	74,41	0,998	3,10
573	300	2,10	77,88	0,998	3,25
623	350	1,93	81,21	0,998	3,38
673	400	1,79	84,40	0,998	3,52
698	425	1,72	85,96	0,998	3,58
723	450	1,66	87,48	0,998	3,65
748	475	1,61	88,98	0,998	3,71
773	500	1,56	90,46	0,998	3,77

Appendix 6: Theoretical Knudsen diffusion

Table 13 – Theoretical Knudsen diffusion permeance calculated for helium and hydrogen.

T (K)	T (°C)	P (µmol/m²·s·Pa)	
		Hydrogen	Helium
273	0	8,58	6,07
323	50	7,89	5,58
373	100	7,34	5,19
423	150	6,89	4,88
473	200	6,52	4,61
523	250	6,20	4,38
573	300	5,92	4,19
623	350	5,68	4,02
673	400	5,47	3,86
723	450	5,27	3,73
773	500	5,10	3,61
823	550	4,94	3,50